Geophys. J. Int. (2004) **156,** 94–114 doi: 10.1111/j.1365-246X.2004.02038.x

Modelling the spatial distribution of present-day deformation in Nepal: how cylindrical is the Main Himalayan Thrust in Nepal?

Antoine Berger,[1] François Jouanne,[1] Riad Hassani[2] and Jean Louis Mugnier[3]

[1]*Laboratoire de Géodynamique des Chaînes Alpines, UMR CNRS* 5025, *Université de Savoie,* 73376 *Le Bourget du Lac, France.*
E-mail: antoine.berger@univ-savoie.fr
[2]*Laboratoire de Géophysique interne et tectonophysique, UMR CNRS* 5559, *Université de Savoie,* 73376 *Le Bourget du Lac, France*
[3]*Laboratoire de Géodynamique des Chaînes Alpines, UMR CNRS* 5025, *Université Joseph Fourier, Maison des Géosciences,* 38041 *Grenoble Cedex, France*

Accepted 2003 May 14. Received 2003 May 9; in original form 2002 July 2

SUMMARY

The structure of the Himalayas in Nepal is characterized by underthrusting of the Indian lithosphere beneath the chain along the Main Himalayan Thrust (MHT). The MHT is affected by major earthquakes of $M > 8$ that have ruptured segments several hundred kilometres in length. The study of historical seismicity underlines the existence of a significant seismic gap between the 1905 Kangra and the 1934 Bihar–Nepal earthquake areas in Western Nepal. This contribution presents a numerical model of the interseismic deformation using the ADELI 2-D finite-element code. A parametric study has been performed to estimate the influence of the topography, the geometry of the flat–ramp–flat transition of the MHT and its rheology. The results of these runs are compared along three cross-sections of Eastern, Central and Western Nepal using various recordings of the active deformation of Nepal (neotectonics, microseismicity, GPS velocities, vertical displacement rates deduced from comparative levellings). The results of this study suggest: (1) a small amount of aseismic slip along the southern part of the MHT and (2) an abrupt change in geometry of the MHT between Central and Western Nepal. The stress build-up in Eastern and Central Nepal is produced by coupling of a bend (flat–ramp transition) of the MHT and a brittle–ductile transition at the foot of the ramp. In Western Nepal, on the other hand, stress build-up is only induced by a brittle–ductile transition located along the low-angle part of the MHT. This difference suggests the presence of a lateral ramp on the MHT to allow transition between the Central and Western Nepal geometries of the MHT. This change in MHT geometries between Central and Western Nepal is also clearly marked in the Himalayan relief: an abrupt decrease in altitude and incision between Central and Western Nepal.

Key words: collision belts, continental deformation, fault models, Himalaya, Nepal, rheology, stress distribution, uplift, viscoelasticity.

INTRODUCTION

Half of the present-day convergence between India and Eurasia is absorbed through the Himalayas by underthrusting of the Indian lithosphere beneath the Himalayas and Tibet along the Main Himalayan Thrust (MHT) as suggested by seismic investigations (Zhao *et al.* 1993). This hypothesis is reinforced by the observation that Quaternary displacement along the Main Frontal Thrust, southern emergence of the MHT and the convergence rate estimated across the Himalayas by GPS are both estimated at 18–20 mm yr^{-1}, which suggests that nearly all the displacement between India and Tibet is transfer, at the geological scale, along the MHT. Many earthquakes have occurred along this basal detachment, the biggest reaching $M > 8$ (Kangra 1905; Bihar 1934). Many studies (Bilham *et al.* 1995; Jouanne *et al.* 1999; Larson *et al.* 1999; Pandey *et al.* 1999) have shown that these earthquakes indicate the existence of a locked zone along the southern part of the Main Himalayan Thrust (underthrust of the Indian lithosphere beneath Tibet) which is released by $M > 8$ major earthquakes. Meanwhile, a 500–800 km long segment of the mountain range between Central Nepal and Dehra Dun in India, has probably not experienced a high-magnitude earthquake over the past 300 yr and possibly not since the 1255 event (Bilham *et al.* 1995). Microseismicity and geodetic investigations both indicate that the Himalayas of Nepal are currently in an interseismic period during which stress and strain are building up. This stress accumulation will be released when a major seismic event occurs along the basal detachment between India and Tibet (MHT).

To gain a better understanding of present-day deformation of the Himalayas, interseismic deformation of the Nepalese Himalayas was simulated. Previous studies have already focused on the

modelling of interseismic deformation (Bilham *et al.* 1997; Jouanne *et al.* 1999; Cattin & Avouac 2000) along a single cross-section. Larson *et al.* (1999) has already compared the deformation of Western and Eastern Nepal by using a dislocation model. The work described here focuses on the difference between several cross-sections of the Himalayan belt in order to characterize the Main Himalayan Thrust geometry and mechanical behaviour for Eastern, Central and Western Nepal. The model boundaries were defined on the basis of geodetic displacements (GPS, levelling), microseismicity data and balanced cross-sections to determine belt geometry, coupled with the results of neotectonics investigations to define the Quaternary shortening rates along the frontal thrusts.

GEOLOGICAL SETTING OF NEPAL

Thrust system geometry and long-term velocity

The geological structure of the Nepalese Himalayas is characterized by several north-dipping thrust faults (Fig. 1): the Main Frontal Thrust, the Main Boundary Thrust, the Mahabarat Thrust and the Main Central Thrust trending generally N120° in Western Nepal to E–W in Eastern Nepal (Upreti & Le Fort 1999). These thrust faults, with generally N–S transport direction (Brunel 1986; Mugnier *et al.* 2003), are generally inferred to branch off the Main Himalayan Thrust, which marks the underthrusting of the Indian lithosphere beneath the Himalayas and Tibet (Zhao *et al.* 1993). Numerous structural cross-sections (Fig. 2) have been made through the Himalayan belt. All of these sections suggest a crustal ramp, below a large-scale antiformal structure of the Lesser Himalayas and to the north of a synformal structure (Schelling & Arita 1991; Srivastava & Mitra 1994; Pandey *et al.* 1999; DeCelles *et al.* 1998; Mugnier *et al.* 2003). The comparison of these sections also indicates considerable differences. Though direct knowledge on the geometry is currently sparse, and therefore details of these sections highly questionable, two types of section are identified: the Western sections with a narrow upper flat (less than 50 km wide) and a shallow ramp (less than 20 km) and the Eastern sections with a large upper flat (more than 70 km wide) and a deep ramp (more than 20 km).

Long-term displacement rates have been estimated from numerous studies (see, for example, Powers *et al.* 1998 or Mugnier *et al.* 2003 for a compilation). A shortening rate of the order of 16–21 mm yr^{-1} has been found. Quaternary displacements are mainly localized along the more frontal thrusts where the displacement rate deduced from the uplift of Holocene terraces is 21.5 ± 2.5mm yr^{-1} in Central Nepal (Lavé & Avouac 2000), 19 ± 6mm yr^{-1} (Leturmy & Mugnier 1998; Mugnier *et al.* 2003) in Western Nepal, 15 ± 3 mm yr^{-1} in Western India (Wesnousky *et al.* 1999). This increase in shortening rate towards the east agrees with the location of the rotation pole between India and Eurasia (27.3°N, 23.0°E, Wang *et al.* 2001), which predicts an eastward increase of convergence rate along the Himalaya.

Seismicity

The high magnitude of Himalayan earthquakes (1905, 1934 and 1950) seems to be due to ruptures along the Main Himalayan Thrust (Molnar 1987). During these events, 200–300 km long segments along-strike and 60–100 km down-dip of the MHT (Pandey & Molnar 1988) are affected by coseismic displacements of 3–10 m (Molnar 1990; Bilham *et al.* 1995; Avouac *et al.* 2001; Mugnier *et al.* 2003). The location of the rupture areas of these large

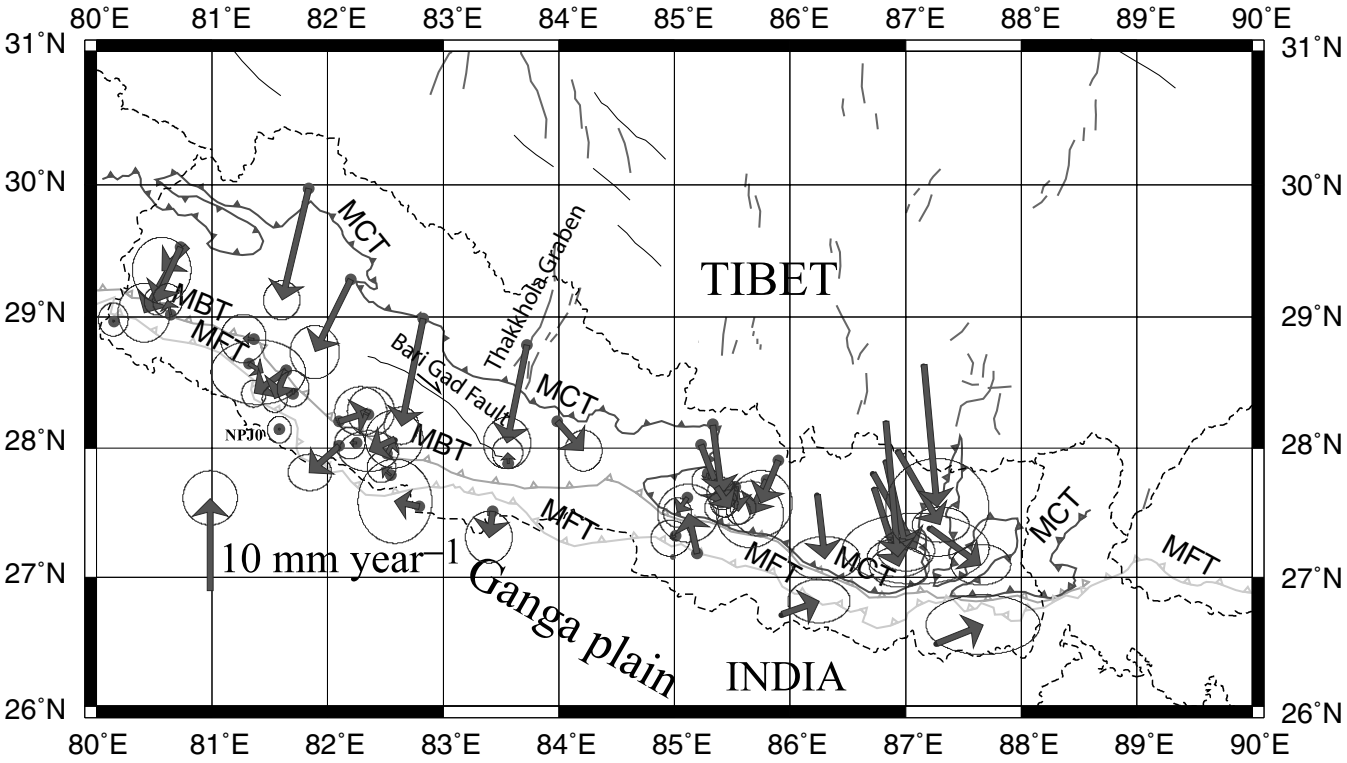

Figure 1. Geological setting of Himalaya of Nepal and South Tibet and GPS velocities. Vectors expressed in the India fixed reference frame Wang *et al.* (2001); Jouanne *et al.* (2003), have been estimated for the 1995–2000 period for the central and western Nepal by Jouanne *et al.* (2003); and for the 1991–1997 period for the eastern Nepal by Wang *et al.* (2001). Error ellipses are drawn for a 95 per cent confidence level.

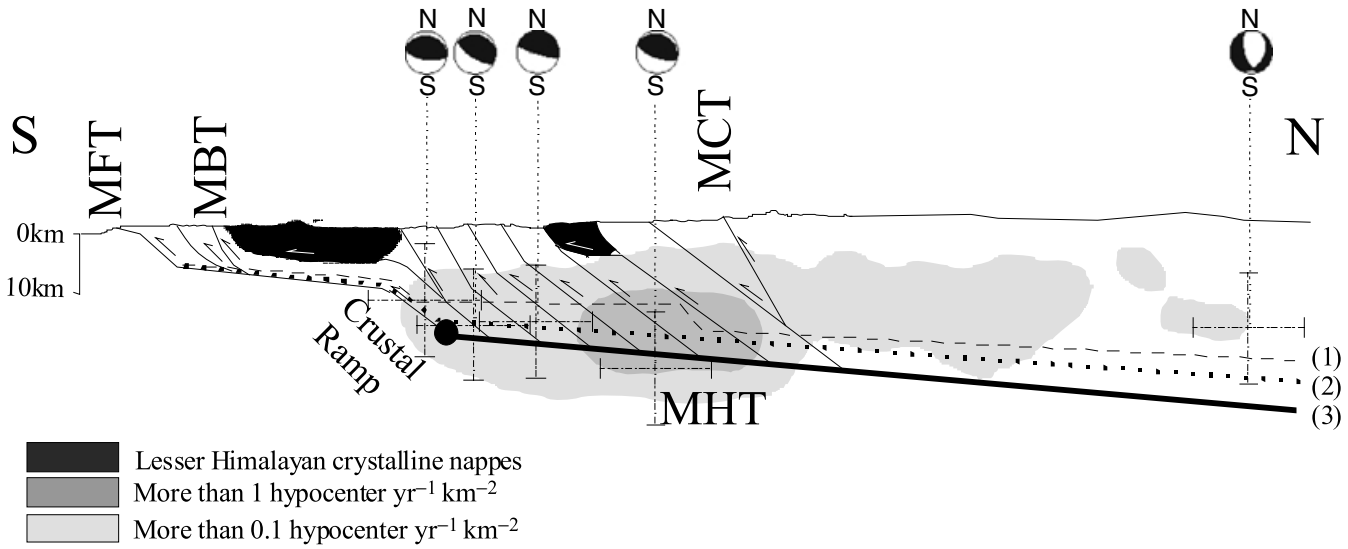

Figure 2. Cross-section established across western Nepal with the projection of microseismic events and of focal mechanisms of medium size earthquakes. Different geometries for the southern part of the Main Himalayan Thrust are indicated: (1) DeCelles *et al.* (1998), (2) DeCelles *et al.* (2001), (3) Mugnier *et al.* (2003).

earthquakes shows a gap along the mountain range between the 1905 Kangra event in India, west of Nepal, and the 1934 Bihar–Nepal earthquake. This region has not experienced such an earthquake probably over the past two centuries and possibly since the huge 1255 event (Bilham *et al.* 1995). Intermediate-magnitude events ($M \sim 5$–7) recorded in the Himalayan–Tibet area occurred at shallow depth (10–20 km) and present focal mechanisms demonstrating the activation of thrust planes gently dipping to the north (CMT solutions, Singh 2000). A detailed study of the $M = 6.6$ Uttarkashi earthquake (Cotton *et al.* 1996), west of Nepal, indicated that this seismic event was initiated at a depth of 12 ± 3km south of the Great Himalayas and corresponded to a southward propagation of the rupture along a 20–25 km segment of the MHT.

Detailed analysis of medium-scale microseismicity demonstrates the existence of several distinct clusters (Pandey *et al.* 1999): in Western Nepal (between longitudes 80.5°E and 82.5°E) the seismic cluster is oriented N118°E, in Central Nepal (between 82.5°E and 86.5°E) N108°E and in Eastern Nepal (between 86.5°E and 88.5°E) N95°E. The projection of these microseismic events along cross-sections reveals a noticeable change in shape of the clusters between Central and Western Nepal (Pandey *et al.* 1999), the Central Nepal cluster has a rounded form and its centre is located near the flat–ramp transition of the MHT, whereas in Western Nepal the cluster is elongated and nearly horizontal.

Present-day deformation

Since 1991, several GPS networks have been installed in Nepal: the Colorado University (CU) network (Bilham *et al.* 1997; Larson *et al.* 1999; Wang *et al.* 2001), the IDYL 1995–1997–1998–2000 networks Jouanne *et al.* (1999, 2003) and the LDG network 1995–1998–2000 Avouac *et al.* (2001); Jouanne *et al.* (2003). These networks have been designed to quantify the present-day deformation across the Himalayan range with points installed from the Ganga plain in the Indian lithosphere to the Tibetan plateau north of the High Range. The CU and the IDYL-LDG networks are linked with seven common points. In this study, focused on the present-day displacements simulation of the Himalayas, we have performed a synthesis of the CU and IDYL-LDG velocity fields. To perform the synthesis of these results and to obtain a readable map, we have expressed the two velocity fields in the India fixed reference frame by subtracting vectors predicted by the Eurasia/India rotation pole from the measured velocity vectors. This transformation has been applied to the Wang *et al.* (2001) and Jouanne *et al.* (2003), velocity fields. This rotation pole (28.5N, 22.1°E, rotation 0.4 deg Myr^{-1}) simulates the displacements, in the Eurasia fixed reference frame, of IISC, Southern India, BRW0, KRN2, MAH0, NIJ0 and NPJ0 in the Ganga plain (Fig. 1).

As shown on Fig. 1, for the seven points common to both networks, there are no significant differences between the two studies, and then no significant distortion between the two velocity sets.

The velocity field (Fig. 1) shows a virtually north–south shortening across the chain, and a progressive attenuation of the displacement towards the south, compatible with strain induced by ductile displacement along the northern part of the MHT, locked south of the High Range Bilham *et al.* (1997); Larson *et al.* (1999); Jouanne *et al.* (1999, 2003). The interseismic displacement pattern and the microseismic distribution are both consistent with segmentation of the MHT particularly between Western and Central Nepal (Jouanne *et al.* 1999; Larson *et al.* 1999). Vertical components of the interseismic displacement field have also been quantified by levelling comparisons along a line crossing the chain at the Katmandu longitude (Jackson & Bilham 1994). Vertical displacement rates, expressed with reference to the Ganga plain, indicate a current uplift of the high chain reaching 6 mm yr^{-1}, but also suggest active displacements along frontal thrusts inducing localized uplift. This last observation suggests that aseismic displacements occurred along frontal thrusts and that the southern part of the MHT may be only partially locked during the interseismic period. Nonetheless, the major seismic events along the Himalayas since the 19th century have released more than 70 per cent of the crustal strain over that period, suggesting that aseismic slip on the MFT cannot account for more than 30 per cent of the total slip (Avouac *et al.* 2001).

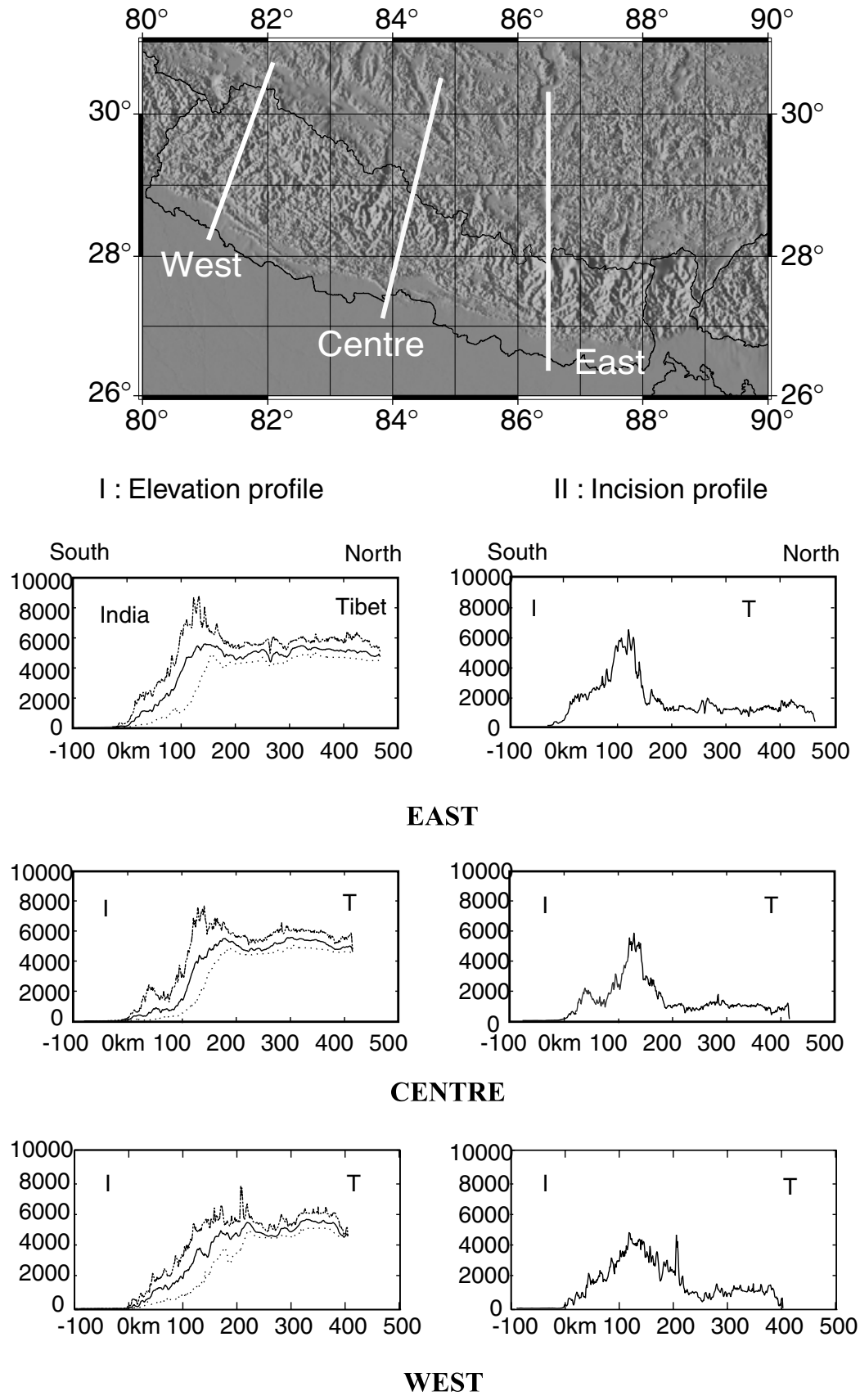

Figure 3. (I) Maximal (up), mean (middle) and minimal (down) elevation profile for eastern, centre and western Nepal; (II) incision profile for eastern, centre and western Nepal. '0 km' position corresponds to the himalayan front (MFT).

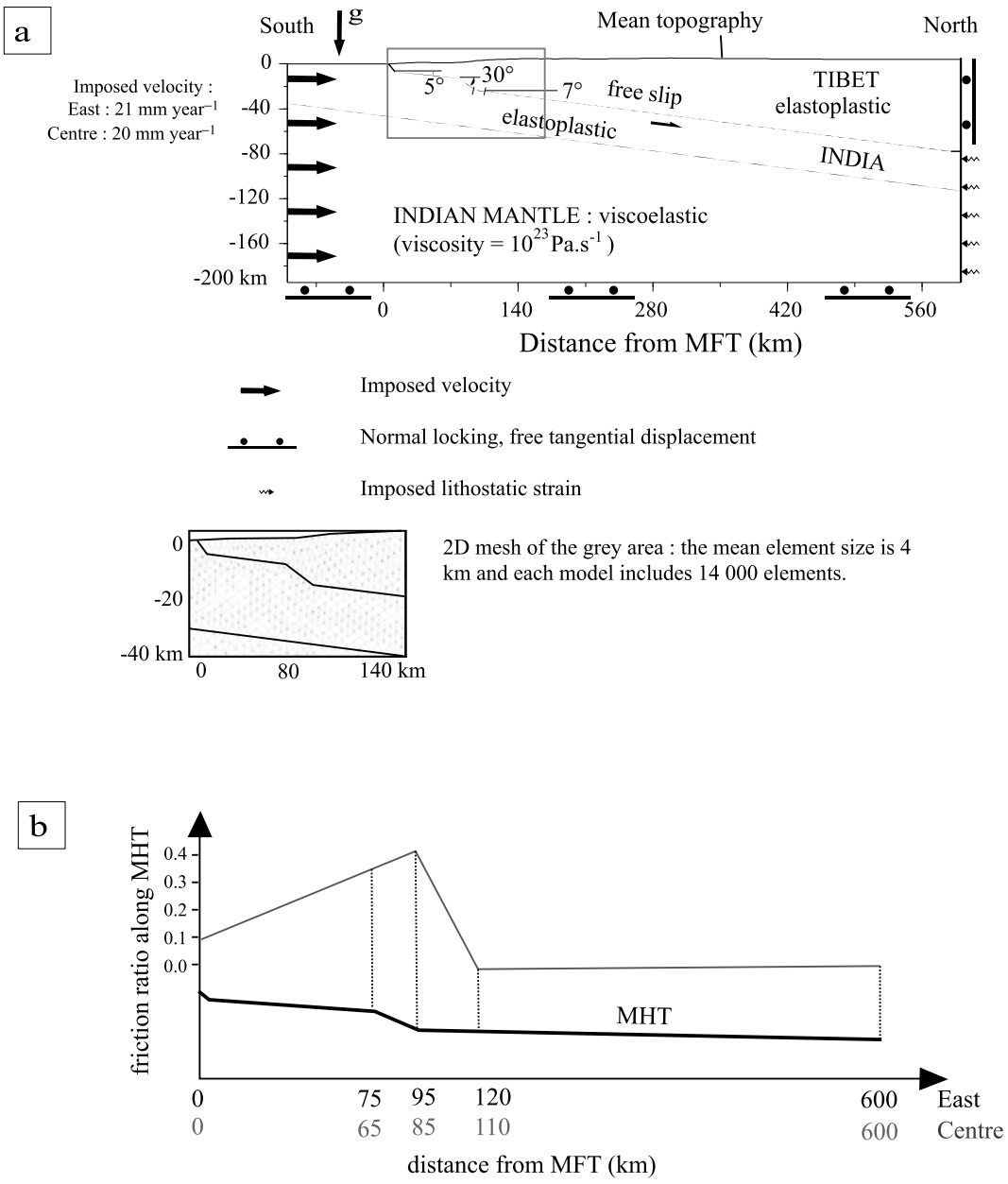

Figure 4. (a) Geometry and boundary conditions of the initial model for eastern and centre Nepal. These two domains are differentiated by the position of the ramp which is 75–95 km/MFT for eastern Nepal and 65–85 km/MFT for centre Nepal. (b) Friction ratios applied on MHT for eastern and centre Nepal models.

Uplift and topography

The Main Himalayan Thrust is the main structure responsible for recent uplifts (Lavé & Avouac 2002) and topography and incision of areas undergoing current deformation is a good marker for long-term vertical displacements (Masek *et al.* 1994). Topographic profiles made perpendicular to the ranges are compared (Fig. 3) in order to illustrate vertical displacement variations along the belt that reveal changes in the geometry of the MHT. The topographic profiles are extracted from a 30 arcsec arc MNT over a 50 km wide stretch perpendicular to the Himalayan front. The maximum, minimum and mean elevations have been extracted as well as incision profiles (the difference between maximum and minimum elevation) for Eastern,

Table 1. Physical and rheological parameters used for the three geological domains: ρ, density; elasticity parameters: E, Young's modulus; ν, Poisson's ratio; η, viscosity; c, cohesion; Φ, internal friction angle; ψ, dilatancy angle.

Parameters	Indian crust	Tibetan crust	Upper mantle
ρ (kg m^{-3})	2900	2700	3350
E(GPa)	90	90	150
ν	0.25	0.25	0.25
η (Pa s)	/	/	10^{23}
c(MPa)	10	10	/
Φ	20°	20°	/
ψ	0°	0°	/

Central and Western Nepal. This analysis shows that for Eastern and Central Nepal, maximum elevation increases suddenly from 0 to 8500 m in an area less than 100 km wide. In the high belt, the mean elevation reaches 5500 m and the incision is greater than 6000 m. The only difference between Eastern and Central Nepal is the presence in Central Nepal of 2000 m elevation mounts in the Himalayan front. In Western Nepal, the elevation does not increase as much, reaching 7500 m in less than 200 km. The mean elevation reaches 5500 m just as in Eastern and Central Nepal. The maximum incision only reaches 4500 m, i.e. 1500 m less than in Eastern and Central Nepal. Moreover, the incision is distributed over a much wider zone in Western Nepal than in Central Nepal. Indeed, the incision area above 2500 m extends over 100 km for Western Nepal and only 60 km for Central Nepal.

The major observation is the reduction in maximum elevation (1000 m) between Central and Western Nepal, and especially the big difference in incision between Eastern–Central Nepal and Western Nepal. This is reflected in a softer relief in Western Nepal and confirms the segmentation of geology and deformation observed with microseismicity and GPS measurements.

SIMULATION OF INTERSEISMIC DEFORMATION

To model interseismic deformation of the Nepal Himalayas, the ADELI 2-D finite-element code (Hassani 1994; Hassani *et al.* 1997) was used. This code was modified to integrate topography and variations in friction coefficient on a discontinuity.

Based on an analysis of seismicity, geodesy and topographical data, Nepal was divided into three distinct zones corresponding to the zones defined by microseismicity, between longitude 89°E and 87°E for Eastern Nepal, 87°E and 83°E for Central Nepal, and between 83°E and 80°E for Western Nepal. For each of these three models, a 700 km long and 200 km depth section was considered in order to cover the entire deformation and to minimize boundary effects. These sections made perpendicular to the earthquake swarm follow a 0°E, 14°E and 20°E direction, respectively, for Eastern Nepal, Central Nepal and Western Nepal.

Each model includes the mean topography calculated above from the DEM, is meshed with 4 km wide triangular mesh, is loaded with gravity body forces and is subjected to the following boundary conditions (Fig. 4):

(i) southern face (Indian plate and upper mantle): a uniform horizontal displacement of 21 mm yr^{-1} for Eastern Nepal and 20 mm yr^{-1} for Central and Western Nepal;

(ii) northern face (Indian crust and upper mantle): a lithostatic stress;

(iii) bottom face of the Indian mantle and northern face of the Tibetan crust: a zero normal displacement. The sufficiently deep bottom of the model (200 km) justifies this boundary condition for the Indian mantle. For the Tibetan crust, this boundary condition is necessary to model the steady state of Tibet.

Rheological behaviour

Three geological domains were taken into consideration: Indian crust, Tibetan crust and upper mantle. The rheologies of these three blocks were assumed to be homogeneous along the models and similar for Eastern, Central and Western Nepal.

Crustal rheology

Elastic domain. At low stress the crust is assumed to deform elastically. A classical linear relation between strain rate d and stress rate tensor is adopted,

$$\frac{D\sigma}{Dt} = 2Gd + \lambda \mathrm{tr}(d)I,$$

where I is the second-order identity tensor and tr is the trace operator. $D\sigma/Dt$ is the Jaumann time derivative of the Cauchy stress tensor used to ensure the objectivity of such a law within the framework of finite strain. This derivative is defined as follows:

$$\frac{D\sigma}{Dt} = \dot{\sigma} - \omega\sigma + \sigma\omega,$$

where ω is the rotation rate tensor.

λ and G are the Lamé parameters, which are linked to Young's modulus, E, and Poisson's ratio, ν. For crustal rocks, these two elastic properties range between 10 and 100 Gpa for E and 0.2–0.3 for ν (e.g. Turcotte & Schubert 1982). In this study and for the results presented below, a mean value of 0.25 is chosen for ν and a value of 90 Gpa is taken for E (see Table 1).

Elastoplastic domain. The elastic behaviour only holds for a given stress range defined by a yield criterion f:

$$f(\sigma) < 0.$$

In order to take into account the increase in yield strength with pressure a Drucker–Prager criterion was chosen,

$$f(\sigma) = J_2(\sigma) + \alpha(\kappa)[I_1(\sigma) - P_0(\kappa)],$$

where

$$I_1(\sigma) = \frac{1}{3}\mathrm{tr}(\sigma)$$

is the mean pressure

$$J_2(\sigma) = \sqrt{\frac{3}{2}\mathrm{dev}\sigma : \mathrm{dev}\sigma}$$

is the deviatoric stress intensity, and

$$\alpha(\kappa) = \frac{6\sin\phi(\kappa)}{3 - \sin\phi(\kappa)}$$

$$P_0(\kappa) = \frac{c}{\tan\phi(\kappa)}$$

where dev σ is the deviatoric part of σ(dev $\sigma = \sigma - I_1(\sigma)$), ':' is the contracted product of two second-order tensors, c is the cohesion, ϕ is the friction angle, which is a function of the plastic strain intensity κ.

In addition, the plastic flow rule giving the plastic strain rate d_p is defined through a plastic potential g,

$$d_p = \lambda_p \frac{\partial g}{\partial \sigma},$$

where

$$g(\sigma) = J_2(\sigma) + \theta I_1(\sigma)$$

and

$$\theta = \frac{6\sin\psi}{3 - \sin\psi}$$

with λ_p being the plastic multiplier and ψ the dilatancy angle.

In our linked geological and geodetic models, the Indian and Tibetan crusts are assumed to obey this elastoplastic behaviour, and

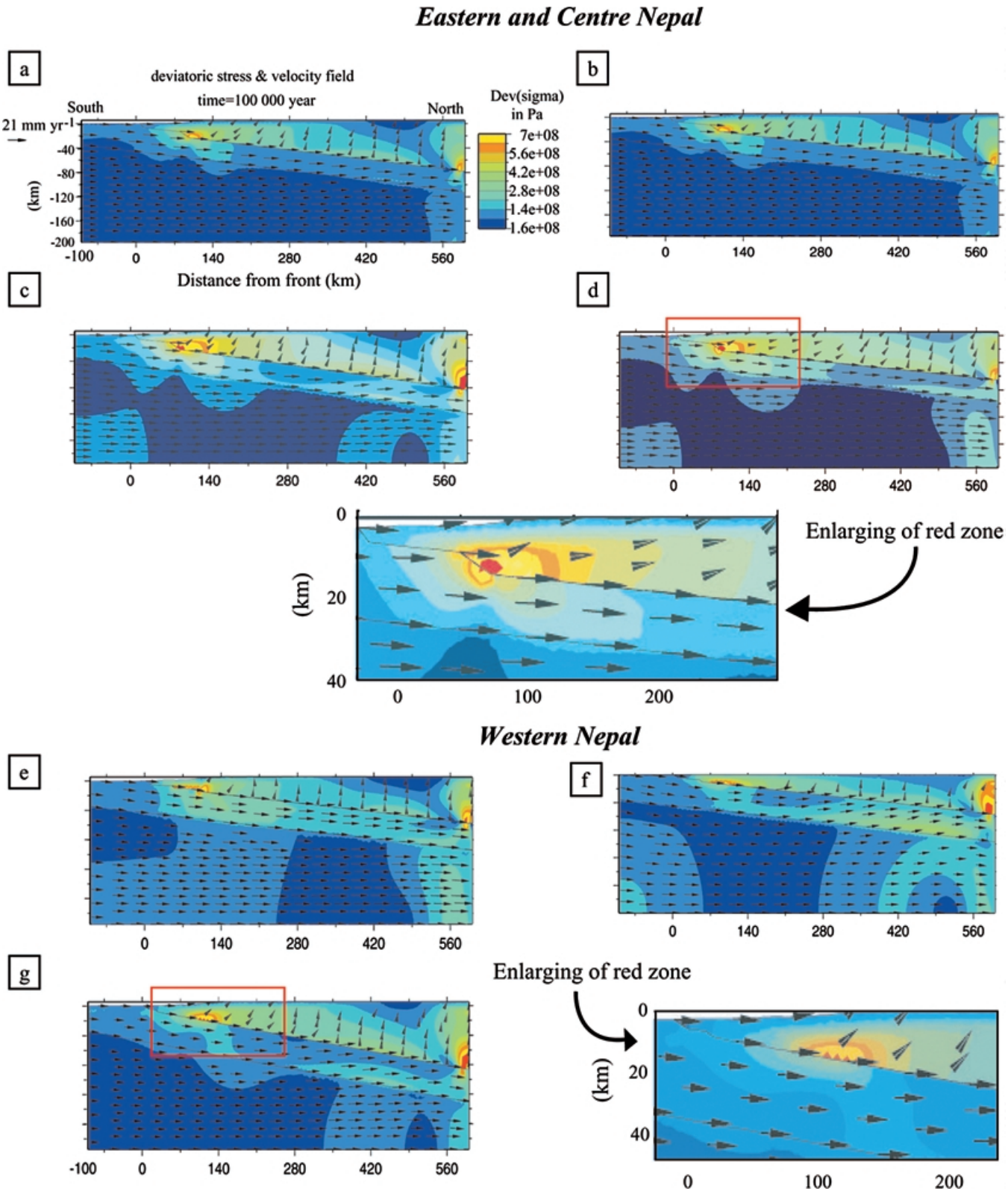

Figure 5. Stress accumulation zones of (a) initial eastern model, (b) initial centre model, (c) final eastern model with a brittle–ductile transition of 10 km width, (d) final eastern model with a brittle–ductile transition of 10 km width, (e) initial western model with two little ramps at 48 and 95 km from front, (f) western model with only one ramp at 48 km from front, (g) final western model.

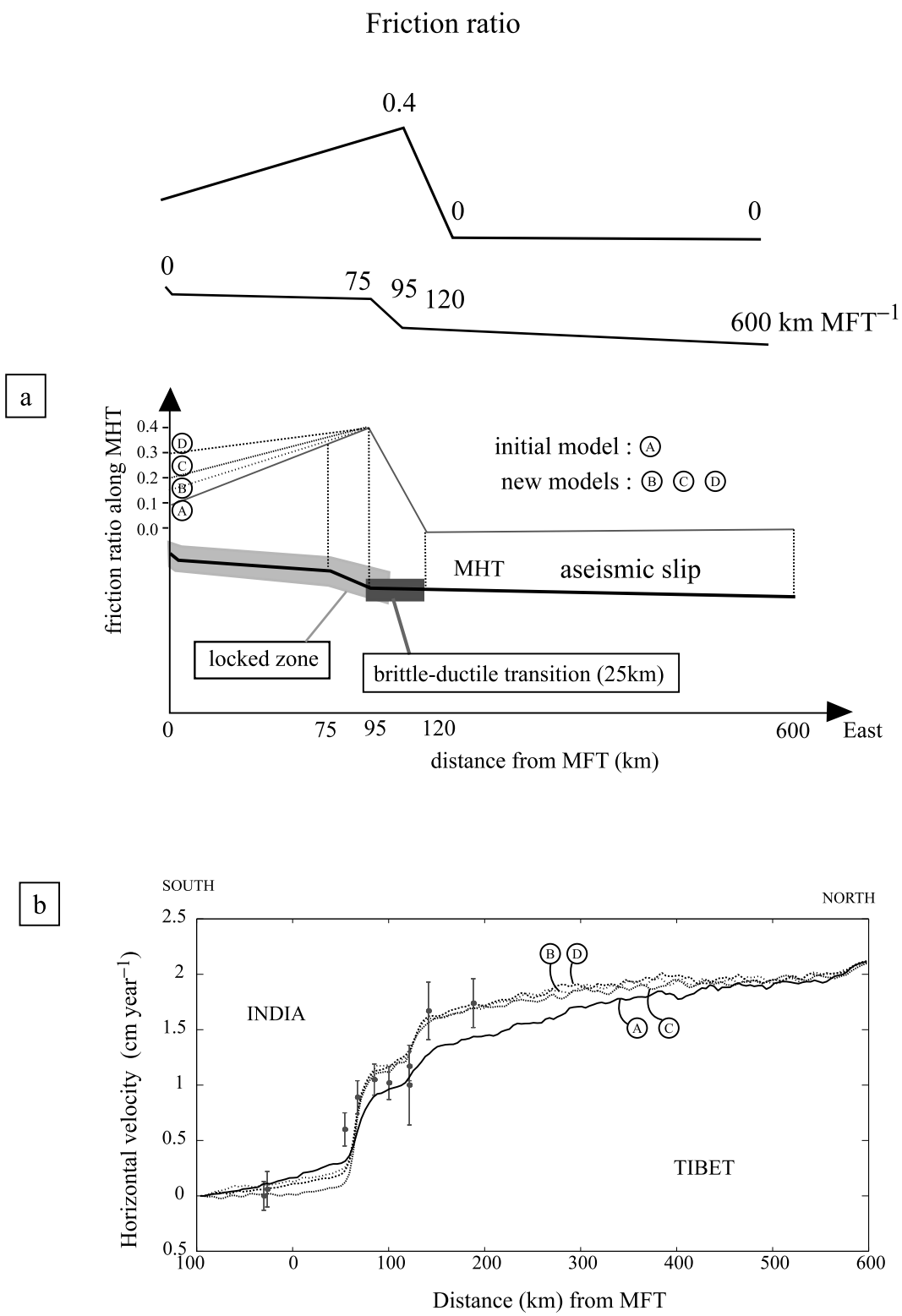

Figure 6. (a) MHT friction ratios for each model accordingly with the distance from the MFT. (b) Calculated (lines) and measured (full circle) interseismic velocities. Measured velocities come from GPS measurements of Wang *et al.* (2001) expressed in the India fixed reference frame with 95 per cent confidence error bars.

we have not investigated model sensitivities to rheological assumptions. Typical values for cohesion and friction angle are listed in Table 1. Regarding the Tibetan crust, the depth of the northern face of the model (80 km) could suggest a viscous rheology in order to take into account the temperature effect at depth. However, the temperature gradient in the Siwaliks ranges is very low (20 deg km^{-1}, Agarwal *et al.* 1994) and there is very little to constrain gradient in the southern part of Tibet (no measurements are available for

southern Tibet north of the studied area). Moreover, if there is a high heat flow in southern Tibet, this area is outside of our principal interest zone (from the Ganga plain to 150 km from the MFT). We use a mean elastoplastic rheology for the entire Tibetan crust to take into account the low heat flow value of the Siwaliks.

Upper-mantle rheology

The rheology of the uppermost mantle is well described by the strain-rate-dependent power law. For the sake of simplicity a linear fit was chosen for this law, i.e. Maxwell's viscoelastic law, where the only new rheological parameter is the viscosity η,

$$\frac{D\sigma}{Dt} = 2Gd + \lambda \mathrm{tr}(d)I - \frac{G}{\eta}\mathrm{dev}\sigma.$$

Typical values of Young's modulus E, Poisson's ratio ν and viscosity η for the upper mantle are used and listed in Table 1.

Although the viscosity is strongly dependent on temperature, a uniform viscosity was chosen in order to keep the model sufficiently simple and easy to interpret. Since the mantle part of the model includes the lithospheric mantle and part of the asthenosphere (Fig. 4a), a mean viscosity of 10^{23} Pa s^{-1} is used. This value is probably too low for the mantle lid, but is too high for the asthenosphere (Cattin *et al.* 2001).

Main Himalayan thrust

Fault behaviour. The frictional contact behaviour between two deformable bodies is assumed to follow the Coulomb law:

$$|\boldsymbol{\sigma}_T| - \mu\sigma_N \leq 0,$$

where $\boldsymbol{\sigma}_T$ and σ_N are the shear stress vector and the normal stress, respectively, on the contact interface (the fault). When sliding occurs, the shear stress vector is given by

$$\boldsymbol{\sigma}_T = -\mu\sigma_N \frac{\mathbf{v}_T}{|\mathbf{v}_T|} \quad \text{for} \quad |\mathbf{v}_T| \neq 0,$$

where $\mathbf{v}_T$ is the sliding velocity vector.

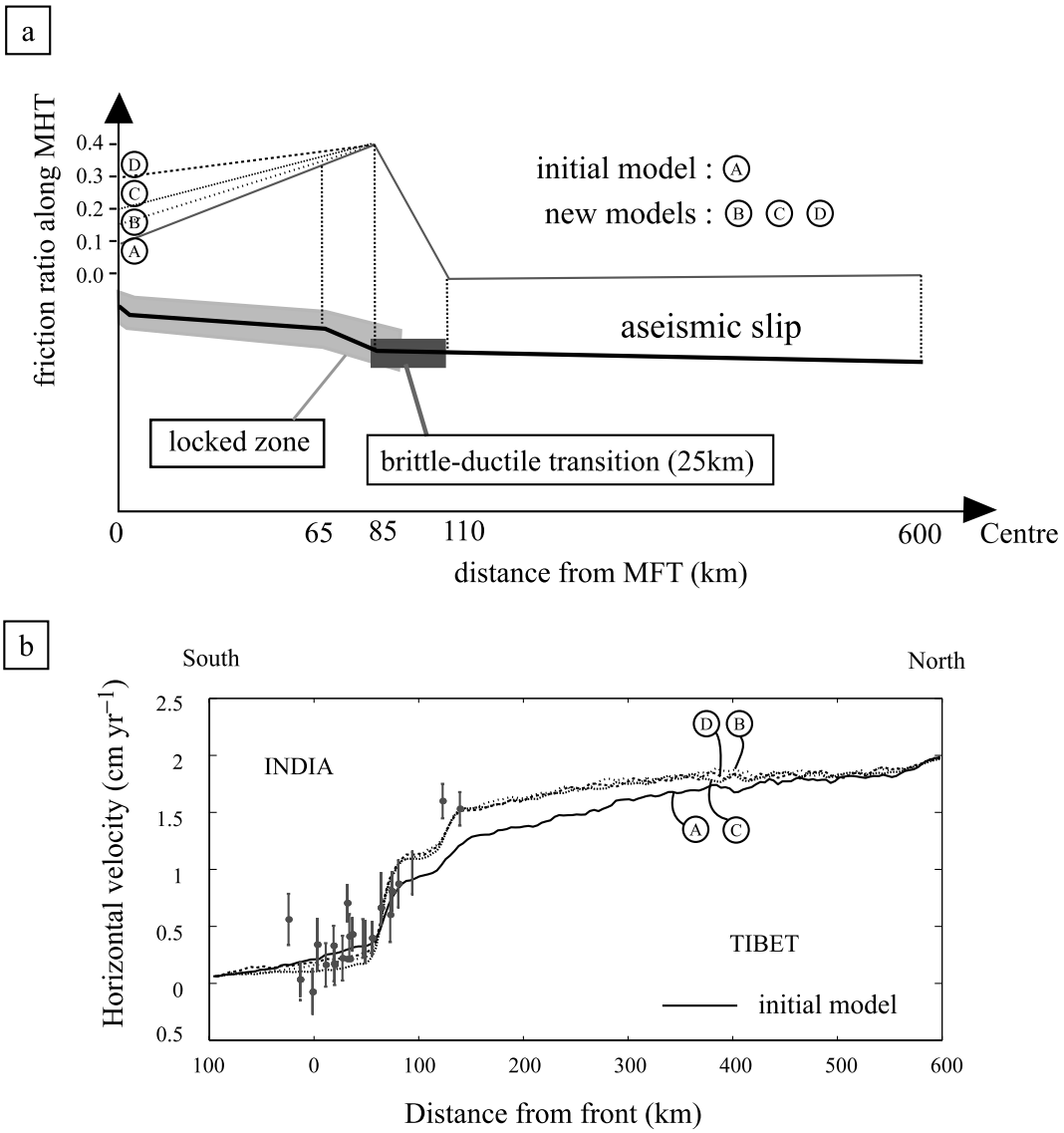

Figure 7. (a) MHT friction ratios for each model accordingly with the distance from the MFT. (b) Calculated (lines) and measured (full circle) interseismic velocities. Measured velocities come from GPS measurements of Jouanne *et al.* (2003) expressed in the India fixed reference frame with 95 per cent confidence error bars.

The only material parameter is the friction coefficient μ, which can vary along the fault.

The convergence between India and Tibet is absorbed along the MHT, which allows underthrusting of the Indian lithosphere beneath the Himalayas and Southern Tibet (Zhao *et al.* 1993). The simulation must then express the displacement along the MHT and then include the variation in friction ratio along this discontinuity. As the friction ratio is dependent on the depth in the brittle domain and on temperature in the ductile domain, a friction ratio was considered which varies on the MHT (Fig. 4) from:

(1) an almost zero value at the Himalayan front to a high value at the foot of the ramp to simulate an increase in the lithostatic load;

(2) a high value at the foot of the ramp to a zero value along the northern flat to simulate a brittle–ductile transition;

(3) and a zero value under Tibet and High chain to represent free aseismic slipping along the MHT, which is assumed to be a ductile shear zone at these *P* and *T* conditions.

This change in friction ratio along the MHT induces a locked zone just north of the crustal ramp and on the southern flat along which the displacement along the MHT is almost zero. This area coincides, at least partially, with the large earthquake rupture zone.

Since our interest is the interseismic period, an initial steady-state solution corresponding to 50 per cent of the loading process is first computed. Shortening is implemented during the last 50 per cent of

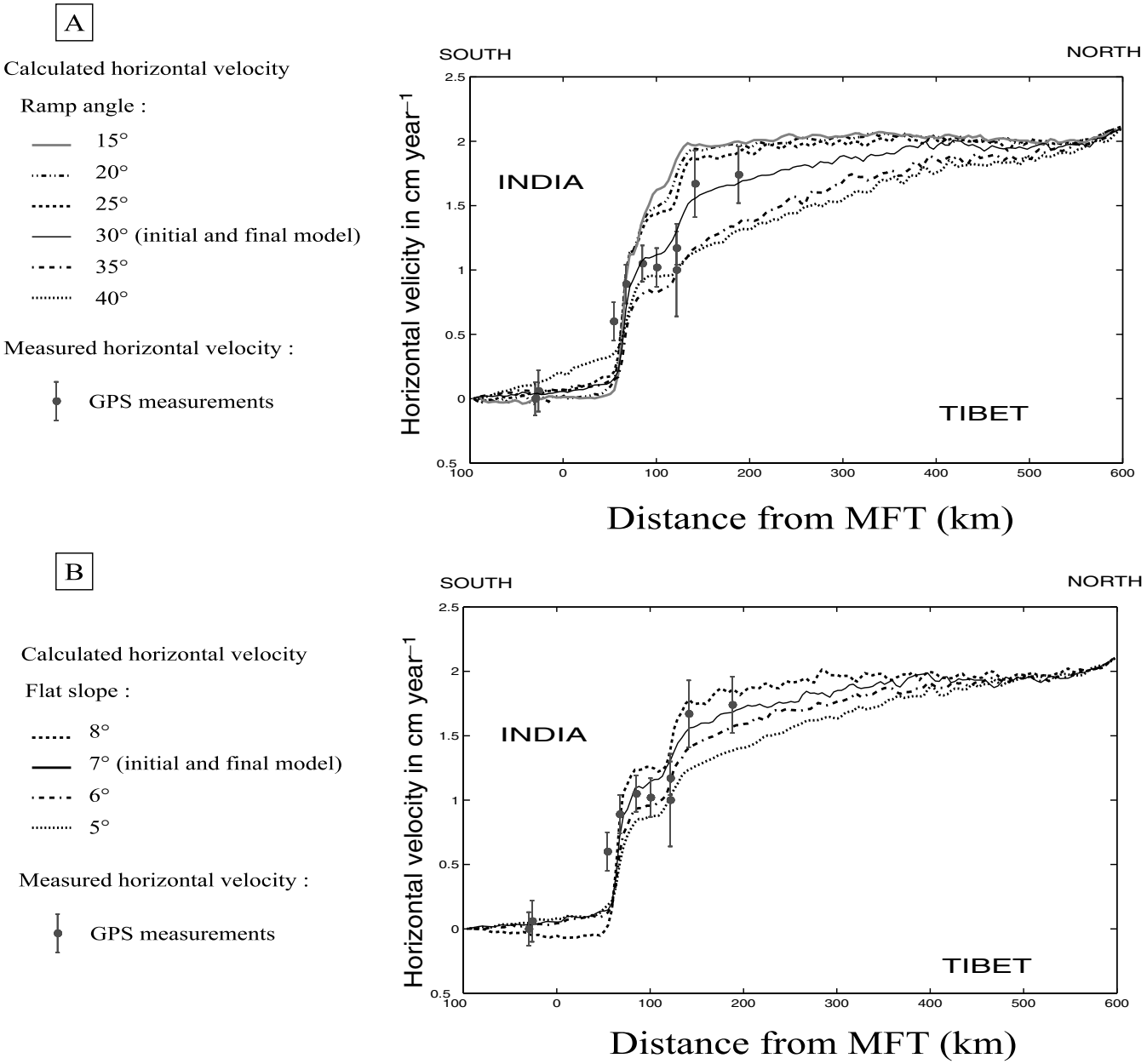

Figure 8. (a) Influence of ramp slope on horizontal velocities for eastern Nepal. (b) Influence of northern flat slope on horizontal velocities for eastern Nepal. Measured horizontal velocities come from GPS measurements of Wang *et al.* (2001) expressed in the India fixed reference frame with 95 per cent confidence error bars.

calculations and averaged instantaneous displacements are plotted on the profile with the Himalayan front as point of origin.

To obtain a better understanding of the interseismic deformation as revealed by geodetic displacements and seismic activity, about 500 different simulations were tested for these three cross-sections, corresponding to different ramp positions, slopes, friction ratio of the MHT, the aim being to find solutions that fit the observed displacements and for which the maximum deviatoric stress accumulation zones are compatible in form and location with the microseismicity clusters assumed to reflect a stress accumulation. In a first result, the model highlights a stress field in agreement with the contrast between Tibet (extensive deformation) and Himalayas (compressive deformation) (Fig. 5) which would appear to support the choice of rheological parameters.

Eastern and Central Nepal model

Initial models for Eastern and Central Nepal

The initial model used for Eastern and Central Nepal resumes the flat–ramp–flat geometry (Brunel 1986; Schelling & Arita 1991; Pandey *et al.* 1999) of MHT (Fig. 4) including a northern flat with 7° dip, a ramp with 30° dip, and a southern flat with 5° dip. For Eastern Nepal, the dip of the Northern flat was estimated using the seismic INDEPTH profile (Zhao *et al.* 1993) and the crustal ramp is assumed to coincide with the earthquake swarm, i.e. between 75 and 95 km from the Main Frontal Thrust. Indeed, if reference is made to the Central Nepal cross-section (Pandey *et al.* 1999), the earthquake swarm is found to be located at the ramp foot, spreading

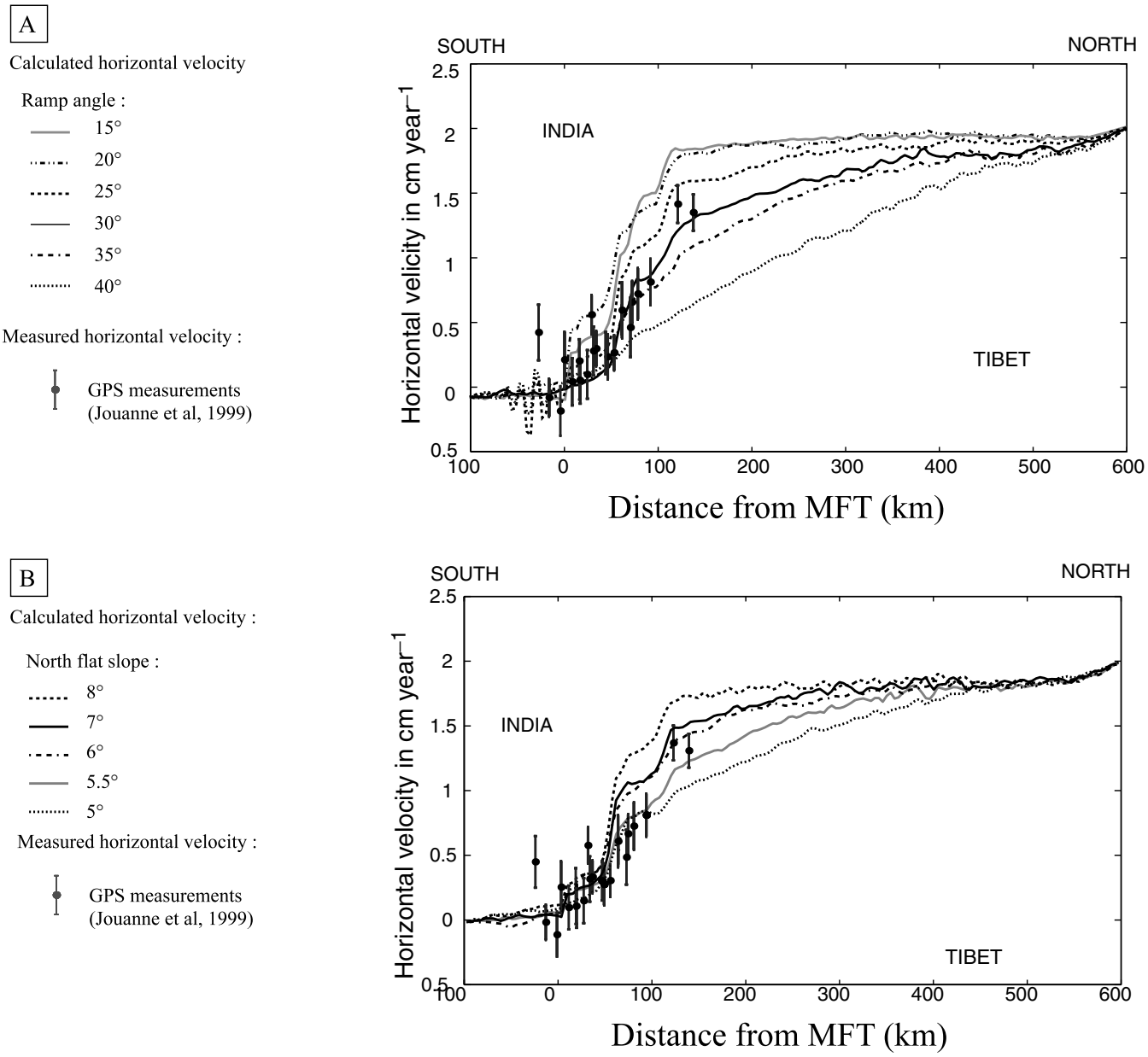

Figure 9. (a) Influence of ramp slope on horizontal velocities for centre Nepal. (b) Influence of northern flat slope on horizontal velocities for centre Nepal. Measured horizontal velocities come from GPS measurements of Jouanne *et al.* (2003) expressed in the India fixed reference frame with 95 per cent confidence error bars.

over the entire ramp. For Central Nepal, the ramp is 10 km further south (between 65 and 85 km from MFT) in accordance with the earthquake swarm and the regional cross-sections (Schelling & Arita 1991; Pandey *et al.* 1999). Finally, a topographic profile, made between 87°E and 88°E longitudes along a north–south line for Eastern Nepal and between 85°E and 86°E longitudes along 14°N line for Central Nepal, was taken into account in the surface model.

As shown on Fig. 4, an elastoplatic rheology was used for the Tibetan and Indian crust and a viscoelastic rheology for the mantle. A velocity was imposed on the southern face: 20 mm yr^{-1} for Central Nepal and 21 mm yr^{-1} for Eastern Nepal. A locked normal velocity was imposed on the northern face of Tibet and at the base of the mantle, and a hydrostatic pressure on the northern face of India and the mantle.

Influence of different parameters

Influence of friction along the upper flat of the MHT. Simulations highlight the fact that the value of the friction ratio along the upper flat controls the shortening pattern above the upper flat, and also in the inner zone of the Himalayas. The initial model of friction ratio (A in Figs 6 and 7) did not give good agreement between observed and simulated horizontal and vertical displacements and between the deviatoric stress accumulation and the microseismicity (Figs 5a and b): the deviatoric stress accumulation zone is located near the foot of the ramp but also along the northern flat of the MHT. The final solutions, providing satisfactory simulations of displacements and deviatoric stress accumulation, have been obtained with an increase in the friction ratio along the southern flat from 0.15 to 0.3 at the

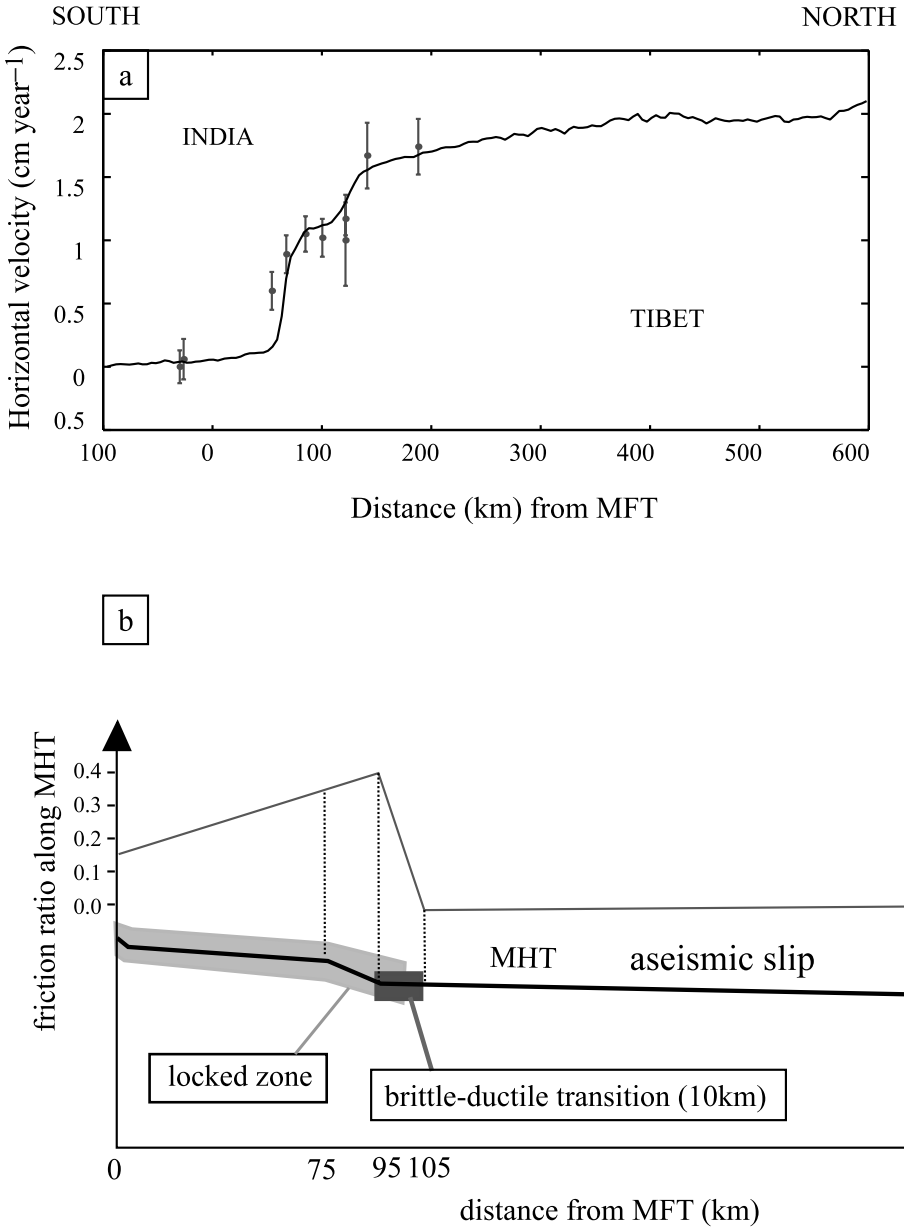

Figure 10. (a) Calculated (lines) and measured (full circle) interseismic velocities for final eastern model. Measured velocities come from GPS measurements of Wang *et al.* (2001) expressed in the India fixed reference frame with 95 per cent confidence error bars. (b) MHT friction ratios for final eastern model accordingly with the distance from the MFT.

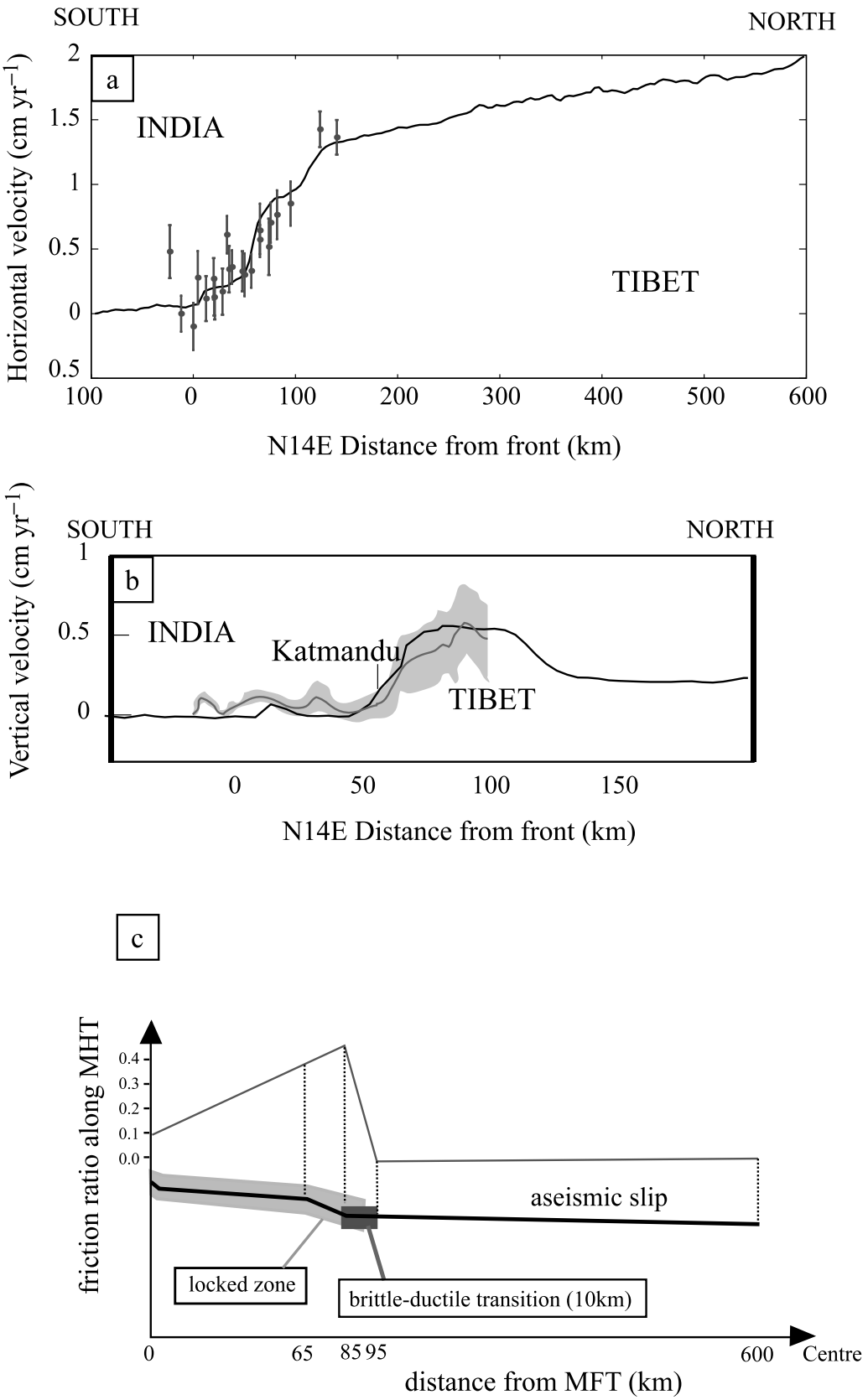

Figure 11. (a) Calculated (lines) and measured (full circle) horizontal interseismic velocities for final centre Nepal model. Measured velocities come from GPS measurements of Jouanne *et al.* (2003) expressed in the India fixed reference frame with 95 per cent confidence error bars; (b) Calculated (black lines) and measured (grey area) vertical interseismic velocities for final centre Nepal model. Measured velocities come from levelling measurements of Jackson & Bilham (1994); (c) MHT friction ratios for final central model accordingly with the distance from the MFT.

southern and northern ends (Figs 6 and 7), an increase along the crustal ramp from 0.3 to 0.4 and a considerable decrease in the friction ratio from 0.4 to 0 near the flat–ramp connection (Figs 6 and 7), suggesting the existence of ductile displacement along the MHT a few kilometres from the crustal ramp. Finally, to be in agreement with the location of the microseismicity cluster, a brittle–ductile transition of 10 km width (instead of 25 km initially) is necessary to simulate a stress accumulation zone centred on the foot of the ramp (Figs 5c and d).

Influence of the dip of the ramp and of northern flat. To validate the new friction model, the influence of MHT geometry on the horizontal velocities was tested. For this purpose, the ramp angle and the northern flat angle were varied between 15° and 40° and between 5° and 7°, respectively. The results (Figs 8 and 9) show that the north–south absorption of velocities is positively correlated with the dip of the ramp and inversely proportional to the value of the northern flat angle. Moreover, 30° for the ramp angle seems to be the best value, thus confirming the initial value inferred from the classical works concerning ramp geometry. On the other hand, for the northern flat angle, the calculated velocities are closer to the measured values with an angle of 5.5° in Central Nepal and 7° in Eastern Nepal.

Preferred models for Eastern and Central Nepal

After 150 simulations, to explore the influence of northern and southern flat geometry, the dip of the ramp, and the variation in friction ratio along the MHT, the final solutions (Figs 10 and 11) present a northern flat with a 7° dip angle for Eastern Nepal and 5.5° angle for Central Nepal, a crustal ramp south of the high chain with a 30° dip angle, and a southern flat below the Lesser Himalayas and Siwaliks with a 5° dip angle. The displacement is not totally locked

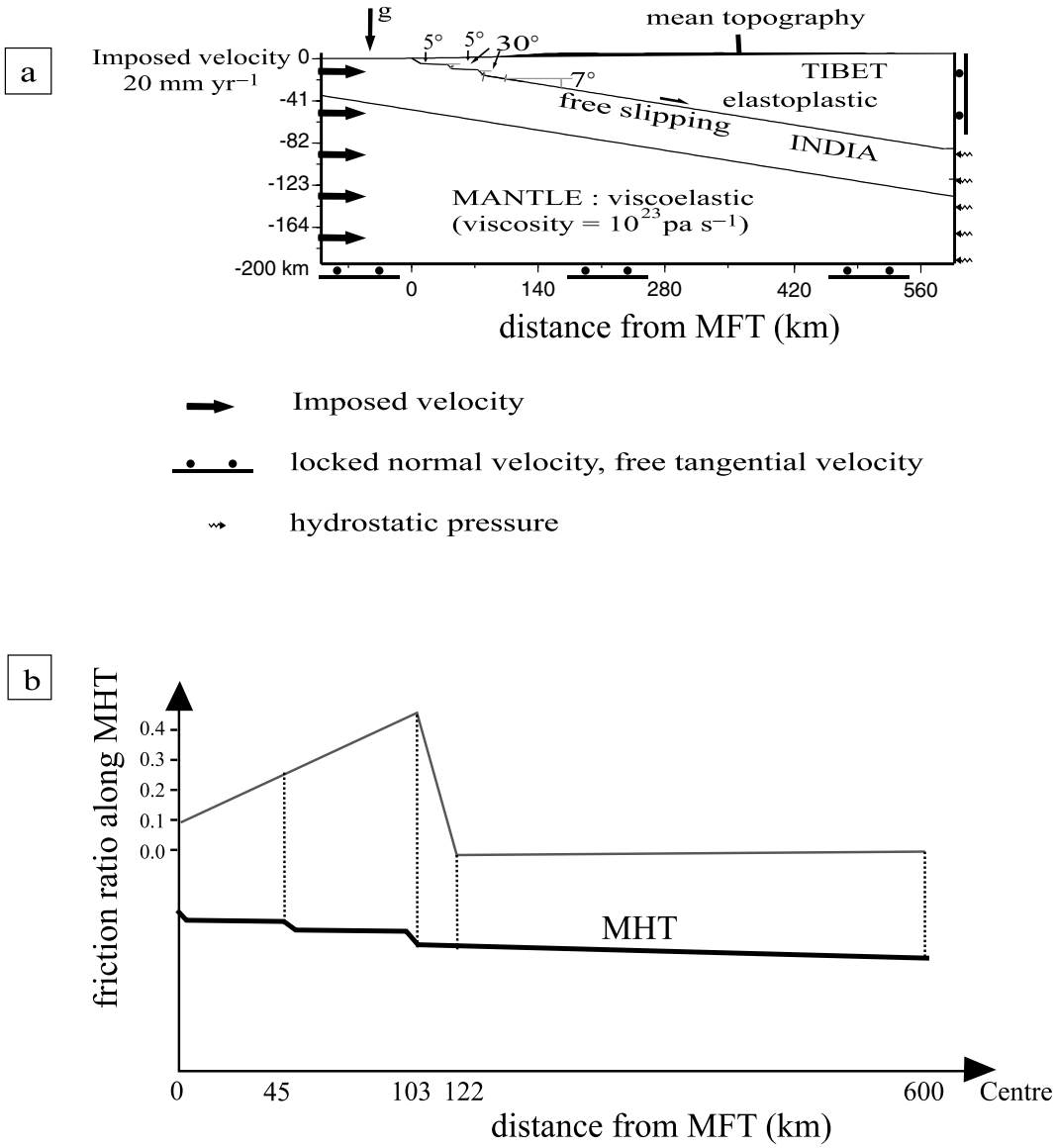

Figure 12. (a) Geometry and boundary conditions of the initial model for western Nepal. (b) Friction ratios applied on MHT for eastern and centre Nepal models.

along the upper flat of the MHT as clearly illustrated by the uplift recorded and simulated to the north of the Main Frontal Thrust, the emergence of the MHT (Fig. 11b). The displacement along the MHT is mainly locked by the ramp–northern flat geometrical transition of the MHT. The simulated deviatoric stress accumulation is in good agreement with the microseismicity cluster located near the northern flat–ramp transition (Figs 5c and d).

Western Nepal model

Initial models for Western Nepal

The initial model of Western Nepal was initially based on the MHT geometry of DeCelles *et al.* (1998). This geometry uses a long flat all along the MHT with a 5° slope on the southern part and a 7° slope on the northern part (Fig. 12). There is no major crustal ramp on this model but only two small ramps 5 km wide with a 30° slope, 48 and 98 km from the front. As for Central Nepal, no geophysical data were available for determining the slope of the MHT flat. Consequently, the INDEPTH value of Eastern Nepal (Zhao *et al.* 1993) was taken as a starting point. A mean topographical profile, made between longitudes 87°E and 86°E along a 20°N line was taken into account.

Finally, the same rheology and boundary conditions as the Eastern and Central models were used, i.e. an elastoplastic rheology for the Tibetan and Indian crust and a viscoelastic rheology for the mantle (Fig. 12). A 20 mm yr^{-1} velocity was imposed on the southern face, a locked normal velocity on the northern face of Tibet and on the base of the mantle, and a hydrostatic pressure on the northern face of India and on the mantle.

Influence of MHT geometry

In order to validate the initial model geometry, the influence of MHT geometry was tested, and especially the importance of small crustal ramps. Three possibilities were tested, the first with two ramps, the second with one ramp (48 km from the front) and the third with no ramp on the MHT. Fig. 13 shows that the presence of a ramp 98 km from the front (initial model) has little influence on the calculated horizontal velocities. Conversely, a lack of ramps induces too small a decrease in horizontal velocities and does not give good simulation of GPS measurements. As regards deviatoric stress accumulation (Fig. 5e), it can be seen that the presence of a second ramp 98 km from the front induces a little disturbance with two stress lobes on each part of this ramp. This result is not in agreement with the regular shape of the microseismicity cluster, and this is why preference was given to the model with only one ramp 48 km from the front. This model is also close to the thrust geometry inferred by DeCelles *et al.* (2001) or Mugnier *et al.* (2003).

The influence of northern flat dip angle was also tested (Fig. 14). In this case, the dip angle was varied between 5° and 9°. The horizontal displacement is weakly sensitive to the dip angle variation, at least for the zone located at a distance greater than 100 km from the front. Nonetheless, a steep dip angle induces low absorption of velocities south up to 100 km from the front. The best result is obtained with a 6° dip angle.

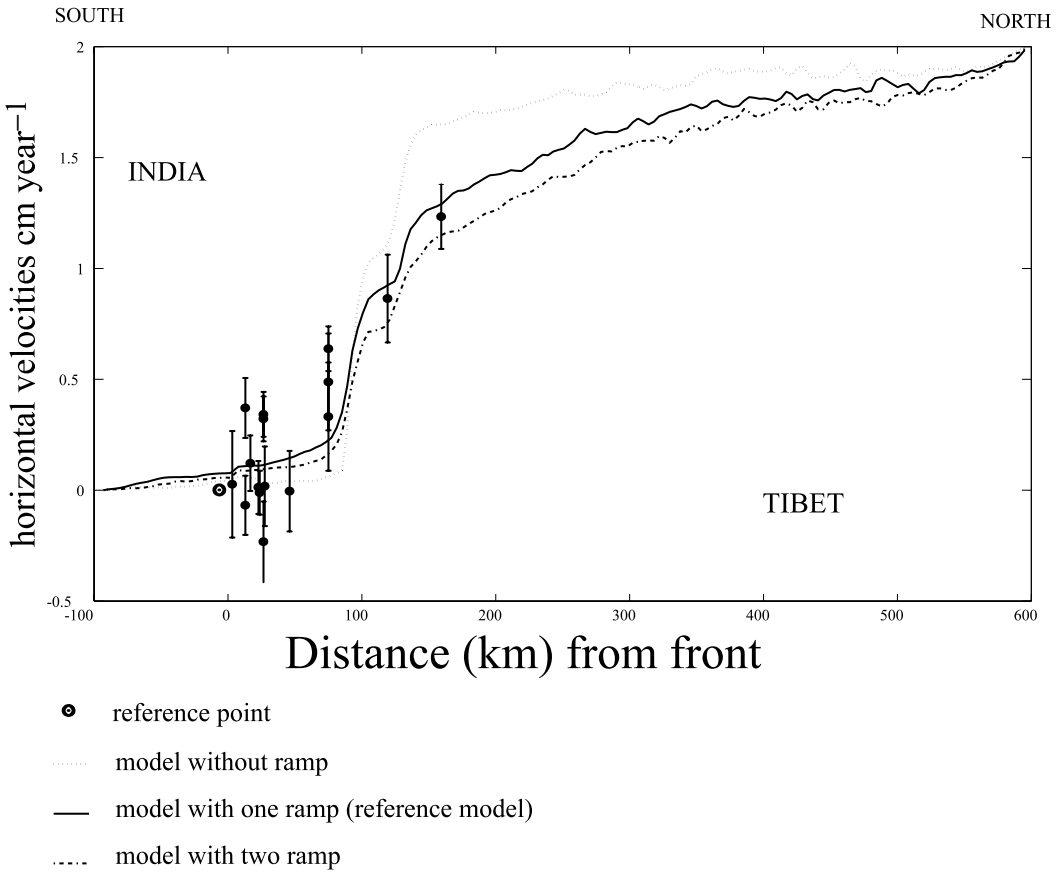

Figure 13. Crustal ramp influence on calculated horizontal velocities for western Nepal. GPS horizontal velocities has been measured by Jouanne *et al.* (2003) expressed in the India fixed reference frame with 95 per cent confidence error bars.

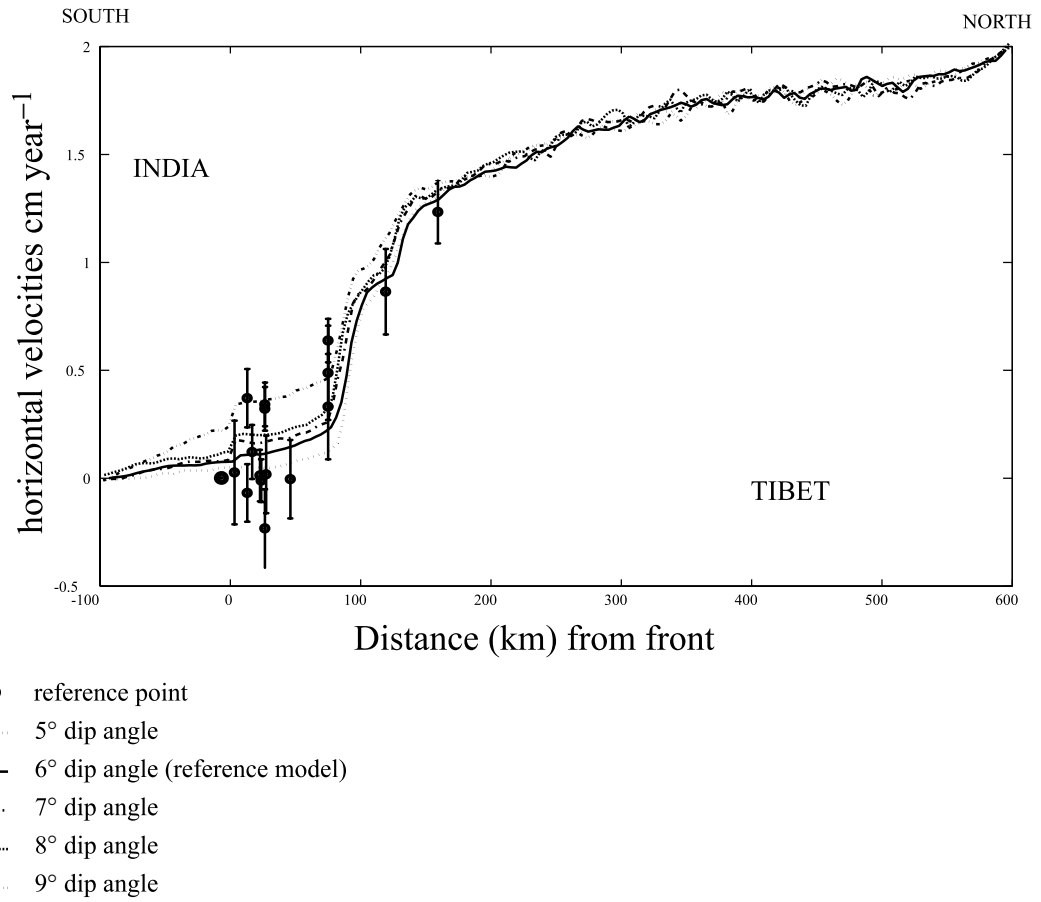

Figure 14. Influence of northern flat dip angle on calculated horizontal velocities for western Nepal. GPS horizontal velocities has been measured by Jouanne *et al.* (2003) expressed in the India fixed reference frame with 95 per cent confidence error bars.

Influence of friction on MHT

This modelling process has shown that friction along MHT has a significant influence on horizontal velocities (Fig. 15). Indeed, from the initial model, it appears that velocities decrease and locked slip is controlled by the brittle–ductile transition between 105 and 115 km from the front. However, the value of friction ratio and width of this transition is very important for the absorption of deformation in agreement with GPS measurements. Fig. 15 shows that the initial 10 km width of the brittle–ductile transition is not sufficient for satisfactory absorption. It also indicates that, even with a 20 km wide transition (between 105 and 125 km from the front), a non-zero friction ratio must be applied at the end of this transition.

Final model for Western Nepal

The best model obtained for Western Nepal is the result of an extensive study of different parameters such as the MHT geometry and the friction ratio of the brittle part of MHT. The final model is quite different from the initial model (Fig. 16). It was obtained using a MHT geometry with only one small ramp 45 km from the front. The slope of the two flats is not particularly different (5° for the southern flat and 6° for the northern flat). The most significant variation relates to the friction ratio under the high belt. Indeed, the brittle–ductile transition is very important in order to obtain a good simulation (see the influence of friction on MHT). This final model presents a wider brittle–ductile transition between 105 and 125 km from the front instead of 105–115 km, with a non-zero friction ratio at a distance of 125 km. The maximum friction ratio reaches 0.42 at 105 km from the front instead of 0.4 initially. Deviatoric stress accumulation (Fig. 5) is well in agreement with the nearly horizontal microseismicity cluster located on the northern flat at a distance of ∼100 km from the front Therefore, it is suggested that this deviatoric stress accumulation and convergence absorption are mainly due to the brittle–ductile transition.

DISCUSSION

Previous studies illustrate that, using a finite-element code, it is possible to obtain geometrical models that simulate interseismic deformation of subduction (Hassani *et al.* 1997) or subduction-like zones (Cattin & Avouac 2001). Referring mainly to active deformation, the present study aims to highlight differences in present-day deformation and MHT geometry between the three zones of Nepal that show distinct geological settings and distinct patterns of active deformation (GPS measurements, levelling, seismicity, active fault, etc.).

Modelling indicates that the differences between Eastern and Central Nepal are really poor. The crustal ramp position is nonetheless offset by ∼10 km, a result already inferred from geological evidence in the initial stage of the modelling. A dip of 6° nearly fits the data set, though the dip angle of the MHT northern flat may be slightly greater in Eastern Nepal than in Western Nepal. These results indicate that Eastern and Central Nepal are bound by the

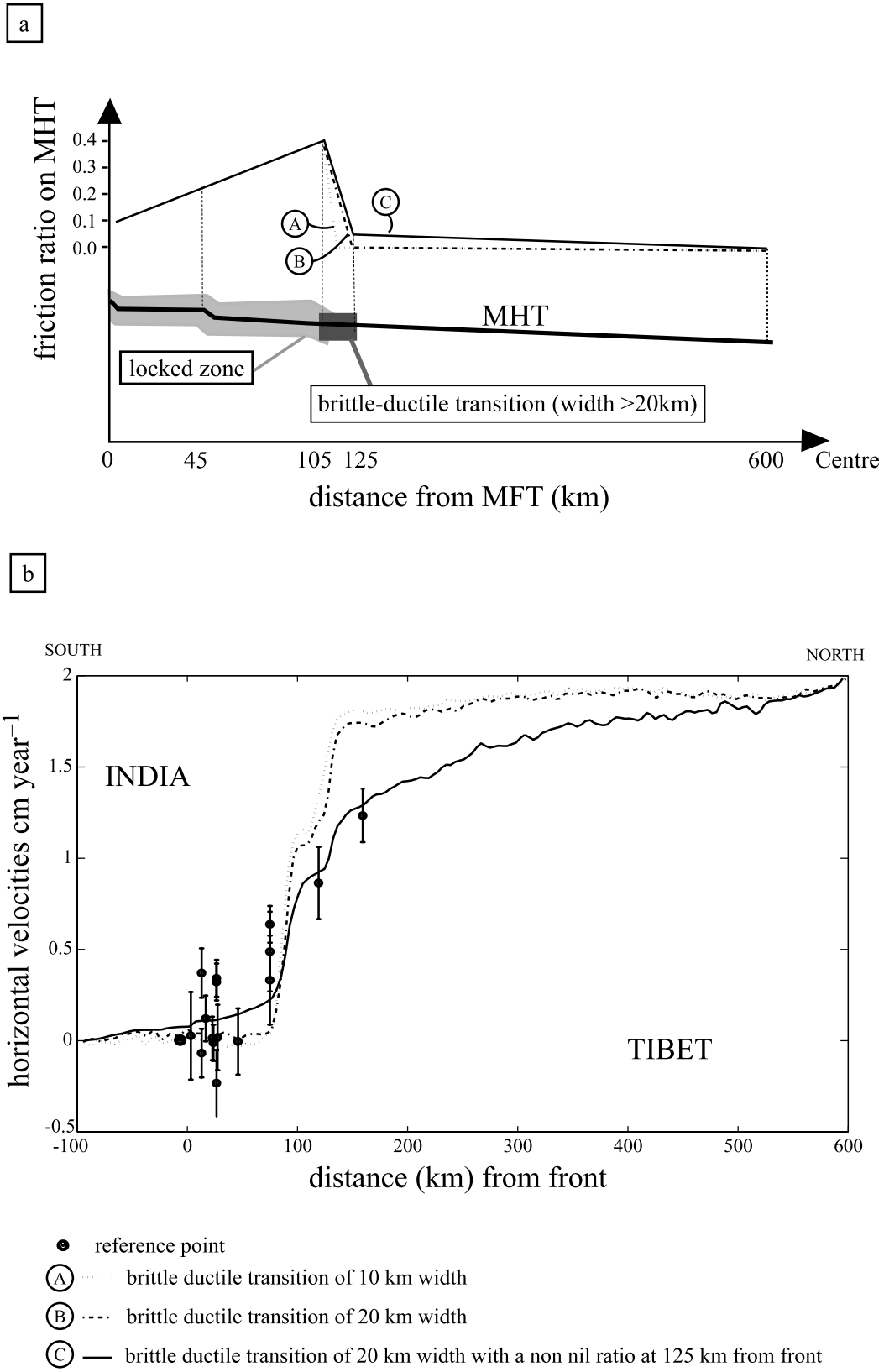

Figure 15. (a) MHT friction ratios for each western model accordingly with the distance from the MFT. (b) Influence of friction along MHT on calculated horizontal velocities for western Nepal. GPS horizontal velocities has been measured by Jouanne *et al.* (2003) expressed in the India fixed reference frame with 95 per cent confidence error bars.

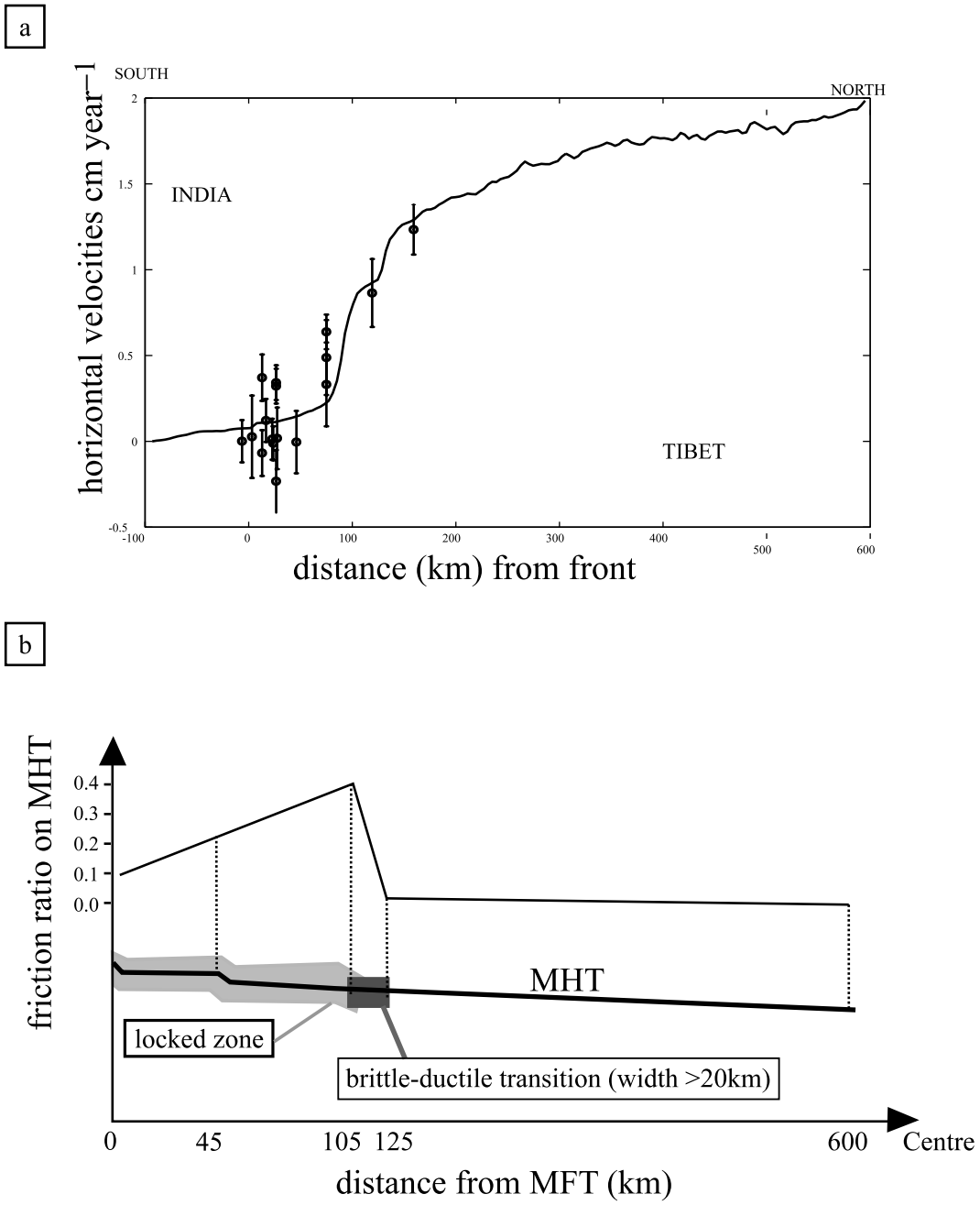

Figure 16. (a) Calculated (lines) and measured (full circle) interseismic velocities for final western model. Measured velocities come from GPS measurements of Jouanne *et al.* (2003) expressed in the India fixed reference frame with 95 per cent confidence error bars. (b) MHT friction ratios for final western model accordingly with the distance from the MFT. This model has been used as a reference model for the influence tests of parameters.

same deformation mode, in order to be in agreement with the microseismicity cluster, and stress accumulation at the foot of the ramp is possible only with a narrow (∼10 km wide) brittle–ductile transition (Fig. 5). This indicates that stress accumulation and locked slipping of the MHT southern flat are caused by coupling of a fault bend (the flat–ramp transition) and a brittle–ductile transition close to the foot of the ramp (less than 10 km to the north). This proximity of the two causes are in agreement with the narrow and rather rounded (in cross-section) microseismicity clusters.

In the case of Western Nepal, in view of the DeCelles *et al.* (1998) MHT geometry without a major crustal ramp, we initially used a geometry with two small ramps on MHT 48 and 95 km from the front. The modelling results show that the presence of a ramp 95 km from the front induces a disturbance of the accumulated stress area that is not in agreement with the microseismicity cluster (Fig. 5), and a model without a small ramp does not simulate the horizontal velocities well. Only the model with a ramp 48 km from the front gives results in agreement with all active deformation markers. Recently, DeCelles *et al.* (2001) proposed a balanced cross-section for Western Nepal with only one small ramp 42 km from the front, which agrees with our final geometry. Our results show that a brittle–ductile transition, more than 20 km wide and far (more than 30 km) from the foot of the ramp, is very important for obtaining a decrease in horizontal velocities (Fig. 15). Our results also indicate that a stress

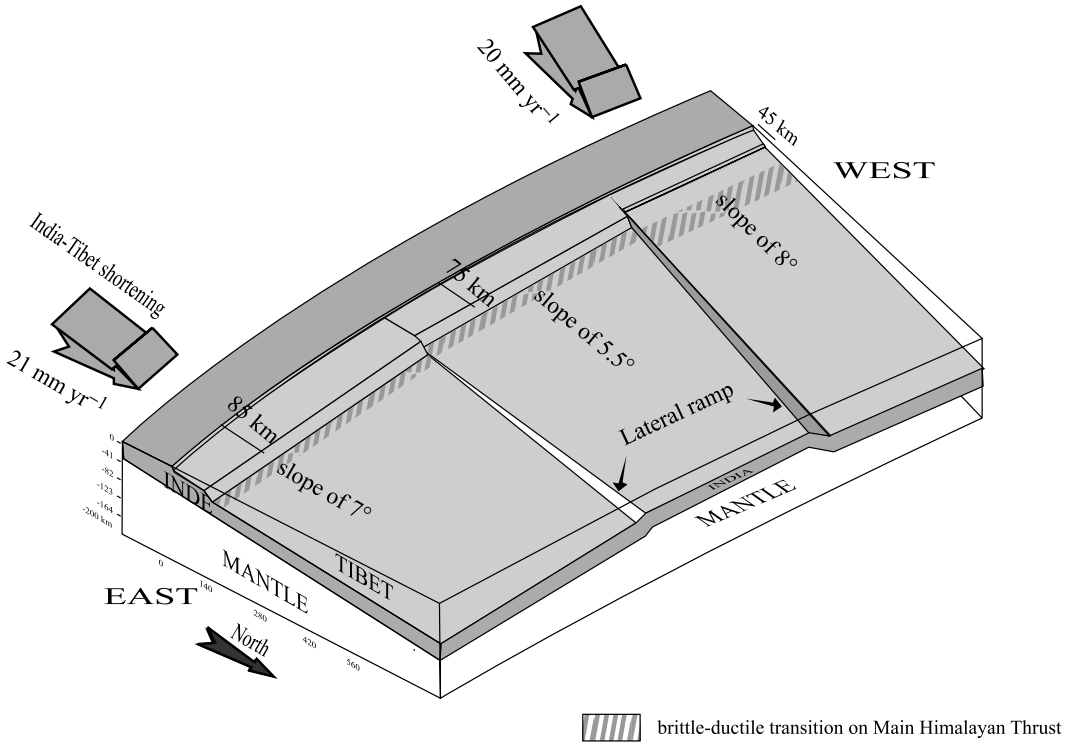

Figure 17. Extension in 3-D of each final model. This interpretation implies brutal changes of geometry between each zones (eastern, centre and western Nepal) and presence of crustal lateral ramps on Indian crust.

accumulation is only obtained, in the absence of a large-scale crustal ramp along MHT, with a wide brittle–ductile transition zone. All of these results confirm that the elongated microseismicity cluster, locking of velocities and deformation in Western Nepal are mainly induced by a wide brittle–ductile transition located along the northern flat of the MHT.

Dragert *et al.* (1994) already pointed out that a wide transition zone develops between the locked and the stable sliding zones of an interplate megathrust. This transition zone may be more precisely defined as the transition from seismogenic velocity-weakening to stable-sliding velocity-strengthening behaviour, and is a part of the seismogenic domain.

During the interseismic period, the attenuation of the sliding in the transition zones occurs by microseismic events and also probably by creeping.

Moreover, most of the intermediate scale ($M \sim 5$–7) seismic events of Nepal occur in western Nepal (Fig. 2). They could either develop along the brittle–ductile transition or south of the transition zone. Cotton *et al.* (1996) points out that the Uttarkashi earthquake in India ($M_w = 6.8$, 1991), located 95 km from the front at a depth of 10–15 km and in the continuity of microseismicity cluster of far-Western Nepal, was caused by a rupture on the portion of the MHT located south of the ductile zone.

The final geometry of the Western Nepal model (no major crustal ramp but a small ramp 48 km from the front and a 6°–8° dip angle for MHT northern flat) gives rise to considerable differences in geometry compared with the models of Central Nepal (major crustal ramp 75 km away, 5.5° dip angle for MHT northern flat) and Eastern Nepal (major crustal ramp 85 km away, 7° dip angle for MHT northern flat). This difference in MHT geometry induces many lateral structural complexities: (1) a difference in dip angle for the northern flat involves lateral discontinuities of the Indian crust because the MHT is not located at the same depth in area; (2) crustal ramps of Eastern and Central Nepal are not located the same distance from the front; and (3) the MHT geometry between Central and Western Nepal is significantly different.

The geological and deformation pattern gives some clues for a better assessment of the lateral complexities of the MHT. Microseismicity can be segmented into three distinct zones (Eastern, Central and Western Nepal), an abrupt change in maximum elevation (break of 1000 m), a considerable difference in incision (more than 1500 m) between Central and Western Nepal, and a considerable difference in the drainage pattern (Van der Beek *et al.* 2002). The abrupt change in geology and relief of the High Himalayas between Central and Western Nepal suggests the presence of lateral ramps on a basal detachment to accommodate the transition of each geometry. These lateral ramps may be the consequence of dislocation of the Indian crust (Faizabad ridge) parallel to the dip orientation of the Indian crust (Raiverman *et al.* 1983).

Fig. 17, based on the combination of geological segmentation and MHT geometry difference in the final models, gives a 3-D sketch of the lateral variation of the Main Himalayan Thrust. This 3-D hypothesis induces: (1) dislocation of the Indian crust by a different dip angle of the MHT northern flat and (2) the likely presence of lateral ramps to accommodate the transition between each northern flat segment and geometry with or without a major crustal ramp.

CONCLUSIONS

Modelling of interseismic deformation of the Himalayas in Nepal has confirmed the role of the major crustal ramp which affects the MHT. This crustal ramp has a dip close to 30°. On the other hand, its location with respect to the front, its extension and the flat dip seem to vary for the three zones of Nepal (east, centre and west) defined by

geological observations. For Eastern and Central Nepal, the MHT presents a flat–ramp–flat geometry similar to the structural model proposed by Brunel (1986). Differences between both these zones are trivial (position of crustal ramp and difference of $1.5^\circ \pm 1^\circ$ for the northern flat dip angle). In these two areas, stress accumulation is caused by coupling of a bend on the MHT (flat–ramp transition) and a brittle–ductile transition close to the foot of the ramp. For Western Nepal, MHT is characterized by a long flat ($7^\circ \pm 1^\circ$ dip angle) with a small ramp 48 km from the Himalayan front. This ramp lies totally in the brittle zone, and stress accumulation is caused by a 25 km wide brittle–ductile transition between 105 and 122 km along the lower flat of the MHT.

For the three areas, the brittle–ductile transition which occurs between 22 and 25 km depth is in agreement with the brittle–ductile transition for continental lithosphere proposed by Le Pichon & Chamot-Rooke (1991) and with the thermic simulation by Cattin & Avouac (2000).

Modelling and geological data suggest that interseismic deformation (i.e. between major earthquakes ($M \sim 8$) of the Himalayas in Nepal) is characterized in Western Nepal by intermediate earthquakes ($M = 5$–7) located between the northern limit of microseismicity clusters and the Himalayan front. They are caused by ruptures a few kilometres wide along the basal detachment (25 km for the $M = 6.8$ Uttarkashi earthquake of 1991, Cotton *et al.* 1996) between the brittle–ductile transition and the foot of the crustal ramp. Therefore, these earthquakes are simply local stress adjustments and do not lead to release of the entire accumulated deformation over interseismic time. For the three areas, the interseismic deformation is also characterized by a small amount of aseismic slip along the southern part of the MHT, which allows us to simulate the uplift affecting the frontal folds during interseismic period as revealed by levelling comparisons, and to understand the existence of aseismic deformation as revealed by structural investigations.

These observations highlight the main difference between earthquakes of intermediate magnitude and those of magnitude (M_o) greater than 8. The high-magnitude earthquakes are caused by a rupture more than 200 km long and 100 km wide (Molnar 1987; Bilham *et al.* 1995), i.e. the entire locked zone of the Main Himalayan Thrust from the ductile zone to the Himalayan front. Consequently, the presence of intermediate earthquakes in the Western seismic gap (west of Katmandu in far Western Nepal) cannot rule out the possibility of major ruptures in Western Nepal.

ACKNOWLEDGMENTS

The authors thank Kristine Larson and Evgeny Burov for their fruitful reviews and comments, and Jean Chéry for helpful comments and suggestions.

REFERENCES

Agarwal, R.P., Prasad, D.N., Samanta, U., Berry, C.M. & Sharma, J., 1994. Hydrocarbon potential of Siwalik basin, in *Siwalik Foreland Basin of Himalaya, Himalayan Geology,* Vol. 15, pp. 301–320.

Avouac, J.P., Bollinger, L., Lavé, J., Cattin R. & Flouzat M., 2001. Le cycle sismique en Himalaya, *C.R. Acad. Sci. Paris,* **333,** 513–529.

Bilham, R., Bodin, P. & Jackson, M., 1995. Entertaining a great earthquake in Western Nepal: historic inactivity and geodetic test for the development of strain, *J. Nepal Geol. Soc., Special Issue,* **11,** 73–88.

Bilham, R., Larson, K., Freymuller, J. & Idylhim members, 1997. GPS measurements of present-day convergence across the Nepal Himalyas, *Nature,* **386,** 1–94.

Brunel, M., 1986. Ductile thrusting in the Himalayas: shear sense criteria and stretching lineations, *Tectonics,* **5,** 247–265.

Cattin, R. & Avouac, J.P., 2000. Modeling mountain building and the seismic cycle in the Himalayas of Nepal, *J. geophys. Res.,* **105,** 13 389–13 407.

Cattin, R., Martelet, G., Henry, P., Avouac, J.P., Diament, M. & Shakya, T.R., 2001. Gravity anomalies, crustal struture and thermo-mechanical support of the Himalaya of Central Nepal, *Geophys. J. Int.,* **147,** 381–392.

Cotton, F., Campillo, M., Deschamps, A. & Rastogi, B.K., 1996. Rupture history and seismotectonics of the 1991 Uttarkashi Himalayas earthquake, *Tectonophysics,* **28,** 35–51.

DeCelles, P.G., Gerhels, G.E, Quade J., Ojha, T.P., Kapp, P.A. & Upretti, B.N., 1998. Neogene foreland basin deposits, erosional unroofing, and the kinematic history of the Himalayan fold-thrust belt, Western Nepal, *Geol. Soc. Am. Bull.,* **119,** 2–21.

DeCelles, P.G., Robinson D.M., Quade, J., Ojha, T.P., Garzione C.N., Copeland P. & Upretti, B.N., 2001. Stratigraphy, structure and tectonic evolution of the Himalayn fold-thrust belt in Western Nepal, *Tectonics,* **20,** 487–509.

Dragert, H., Hyndam, R.D., Rogers, G.C. & Wang, K., 1994. Current deformation and the width of the seismogenic zone of the northern Cascadia subduction thrust, *J. geophys. Res.,* **99,** 653–668.

Hassani, R., 1994. Modélisation numérique de la déformation des systèmes géologiques, *PhD thesis,* Université Montpellier 2.

Hassani, R., Jongmans, D. & Chéry, J., 1997. Study of plate deformation and stress in subduction processes using two-dimensional numerical models, *J. geophys. Res.,* **102,** 17 951–17 965.

Jackson, M. & Bilham, R., 1994. Constraints on Himalayas deformation inferred from vertical fields in Nepal and Tibet, *J. geophys. Res.,* **99,** 13 897–13 912.

Jouanne, F., *et al.*, 1999. Oblique convergence in the Himalayas of Western Nepal deduced from preliminary results of GPS mesurements, *Geophys. Res. Lett.,* **26,** 1933–1936.

Jouanne, F., Mugnier, J.L., Gamond, J.F., Le Fort, P., Pandey, M.R., Bollinger, L., Flouzat, M. & Avouac, J.P., 2003. Current shortening across the Himalayas of Nepal, *Geophys. J. Int.,* in press.

Larson, K., Burgmann, R., Bilham, R. & Freymuller, J., 1999. Kinematics of the India–Eurasia collision zone from GPS measurements, *J. geophys. Res.,* **104,** 1077–1093.

Lavé, J. & Avouac, J.P., 2000. Active folding of fluvial terraces across the Siwaliks Hills, Himalayas of Central Nepal, *J. geophys. Res.,* **105,** 5735–5770.

Lavé, J. & Avouac, J.P., 2002. Fluvial incision and tectonic uplift across the Himalayas of Central Nepal, *J. geophys. Res.,* **106,** 26 561–25 593.

Le Pichon, X. & Chamot-Rooke, N., 1991. Extension of continental crust, in *Controversies in Modern Geology,* pp. 313–338, Academic, New York.

Leturmy, P. & Mugnier, J.L., 1998. Holocene tectonics deduced from incision rates in the seismic gap of the Outer Himalayas, *Int. Symp. on the Origin of Sedimentary Basins,* Oliana, Spain, Abstract, p. 21 Sept. 26–30, 1998. Institut Cartographic de Catalunya, Spain.

Masek, J., Isacks, B., Gubbels, T. & Fielding, E., 1994. Erosion and tectonics at the margin of continental plateaus, *J. geophys. Res.,* **99,** 13 941–13 956.

Molnar, P., 1987. The distribution of intensity associated with the 1905 Kangra earthquake and bounds on the extent of the rupture zone, *J. Geol. Soc. India,* **29,** 221–229.

Molnar, P., 1990. A review of the seismicity and rates of active underthrusting and deformation at the Himalaya, *J. Himalayan Geol.,* **1,** 131–154.

Mugnier, J.L., Huyghe, P., Leturmy, P. & Jouanne, F., 2003. Episodicity and rates of thrust sheet motion in Himalayas (Western Nepal), in *Thrust Tectonics and Hydrocarbon Systems,* McClay, AAPG Mem.

Pandey, M.R. & Molnar, P., 1988. The distribution of intensity of the Bihar Nepal earthquake of 15 January 1934 and bounds on the extent of the rupture, *J. Nepal Geol. Soc.,* **5,** 22–44.

Pandey, M.R., Tandukar, R.P., Avouac, J.P., Vergne, J. & Héritier, Th., 1999. Seismotectonics of the Nepal Himalayas from a local seismic network, *J. Asian Earth Sci.,* **17,** 703–712.

Powers, P.M., Lillie, R.J. & Yeats, R.S., 1998. Structure and Shortening of the Kangra and Derha Dun reentrants, Sub-Himalaya, India, *Geol. Soc. Bull.,* **110,** 1010–1027.

Raiverman, V., Kunte, S. & Mukherjea, A., 1983. Basin geometry, Cenozoic sedimentation and hydrocarbon prospects in North Western Himalayas and Indo-gangetic plains, *Petroleum Asia J.,* **6,** 67–92.

Schelling, D. & Arita, K., 1991. Thrust tectonics, crustal shortening and the structure of the Far-Eastern Nepal Himalayas, *Tectonics,* **10,** 851–862.

Singh, D.D., 2000. Seismotectonics of the Himalayas and its vicinity from centroid-moment tensor (CMT) solution of earthquakes, *J. Geodyn.,* **30,** 507–537.

Srivastava, P & Mitra, G., 1994. Thrust geometries and deep structure of the outer and lesser Himalayas Kumaon and Garhwal (India): implications for evolution of the Himalayas, *Tectonics,* **13,** 89–109.

Turcotte, D.L. & Schubert, G., 1982. *Geodynamics. Applications of Continuum Physics to Geological Problems,* Wiley, New York.

Upreti, B.N. & Le Fort, P., 1999. Lesser Himalayan crystalline nappes of Nepal: problem of their origin, *J. Asian Earth Sci.* (*Advances on the geology of the Himalaya, focus on Nepal geology*) Vol. 17, pp. 577–606.

Van der Beek, P.A., Champel, B. & Mugnier, J.L., 2002. Drainage development in regions of active fault-propagation folding controlled by detachment dip, *Geology,* **30,** 471–474.

Wang, Qi *et al.*, 2001. Present-day crustal deformation on China constrained by GPS measurements, *Science,* **294,** 574–577.

Wesnousky, S., Kumar, S., Mohindra, R. & Thakur V., 1999. Uplift and convergence along the Himalayan Frontal Thrust of India, *Tectonics,* **18,** 967–976.

Zhao, W., Nelson, K.D. & project INDEPTH Team, 1993. Deep seismic reflection evidence for continental underthrusting beneath southern Tibet, *Nature,* **366,** 557–559.